Charge transfer and radiative dissociation dynamics in fluorine-doped solid krypton and argon

H. Kunttu, J. Feld, R. Alimi, A. Becker, and V. A. Apkarian
Department of Chemistry, Institute for Surface and Interface Science, University of California, Irvine, California 92717

(Received 7 November 1989; accepted 10 January 1990)

The photodissociation of F_2 in crystalline Kr is subject to only a minor cage effect—quantum yield of 0.5 at 308 nm, at $T = 12$ K. Two-photon-induced harpooning in the same system leads to dissociation with near unit quantum efficiency; it is shown that this absorption is coherent with a giant cross section of $3(\pm 2)\times 10^{-45}$ cm^4 s at 275 nm. Excitation and emission spectra of charge-transfer transitions in solid Kr doped with F atoms, and solid Ar multiply doped with F/Kr are reported. The vertical excitation in F/Kr leads to a state delocalized over immediate neighbors—assigned to $Kr_6^+ F^-$. This state localizes on a subpicosecond time scale to the triatomic $Kr_2^+ F^-$ configuration. The latter relaxes radiatively ($\tau_r = 140$ ns), to the repulsive wall of the ground state (~ 1 eV above ground). The excitation in F:Kr/Ar solids shows the diatomic KrF($B \leftarrow X$) resonances. From the analysis of the spectrum, a harmonic frequency $\omega = 75(\pm 3)$ cm^{-1} is extracted for F atoms in the ground state, consistent with molecular-dynamics simulations of an octahedrally trapped F atom [$\omega = 70(\pm 1)$ cm^{-1}]. The diatomic KrF(B) state relaxes on a time scale of 20 fs $< t <$ 500 fs to the mixed triatomic configuration, $(ArKr)^+F^-$, which then relaxes radiatively ($\tau_r = 60$ ns). The kinetic energy released upon the radiative dissociation of triatomic exciplexes generates acoustic waves, and defects, and leads to mass transport. The modes of propagation of the acoustic waves, their subsequent thermalization, and self-annealing of the solid, are directly monitored by spatially and temporally resolved transient scattering experiments. A transient loss ($\sigma \cong 10^{-17}$ cm^2), the origin of which is not fully understood, is observed for Kr_2F isolated in solid Kr. The mass transport, and long-range migration of F atoms (~ 10 lattice sites), is directly monitored in multiply doped Ar solids in which the shuttle of F atoms between Xe and Kr centers can be demonstrated.

I. INTRODUCTION

Halogen-doped rare-gas solids (X/RGS) are used as model systems for studies of solid-state charge-transfer energetics and photodynamics. These systems are chosen due to their conceptual simplicity—simple enough to lead to rigorous descriptions of the elementary photophysics, yet varied enough to be able to test the degree of our understanding of the controlling many-body interactions. In this paper, we illustrate this assertion through a detailed study of fluorine-doped solid krypton and argon. An attempt is made to present a rather complete picture of the system and the relevant photoprocesses—characterization of the elementary optical excitations, and all of the subsequent electronic and nuclear relaxation phenomena. The *in situ* photogeneration of F atoms by photodissociation, and photon-induced dissociative charge transfer in F_2/RGS, is the starting point in the experiments. Spectroscopic studies in the atomic F/RGS are used to describe the energetics of both the neutral and ionic interactions between fluorine atoms and the rare-gas solid. The potentials derived from such analyses are used to rationalize both photomobility, and thermal diffusion of atoms. Pump-probe studies are used to characterize the radiative dissociation of charge-transfer states, and the modes of accommodation of the excess energy released in this process by the lattice. In the rest of this introduction, we provide the context in which these issues present themselves.

In a series of earlier papers,[1–4] it has been demonstrated that the vertically accessed charge-transfer states of solid xenon doped with atomic halogens are extensively delocalized, and yield themselves to a description in terms of a Rydberg hole progression.[4] Such delocalized states are metastable; they relax by coupling to phonons to form molecular charge-transfer configurations.[2] The coexistence of both extended and molecular charge-transfer states in the same solid leads to interesting dynamics: charge separation and energy storage, hole migration, and ion-hole recombination are examples.[3] None of these effects are observed in F/Kr solids. Based on excitation spectra, it will be argued that the vertically accessed charge-transfer state in this case is only partially delocalized—delocalization among nearest neighbors only. Such states are well described by the diatomics in ionic systems (DIIS) formalism, which was originally advanced for treating charge-transfer states in Xe.[5–8] Based on the realization that charge-transfer states of X/RGS can be regarded as ion-hole pairs; the trend, that the extent of delocalization would be reduced in going from heavier to lighter rare gases, was anticipated.[4] This, in effect, is the opposite trend of the more traditional excitonic states of ion-electron pairs in rare-gas solids, for which an evolution from the Wannier–Mott to the Frenkel limits in going from Ne to Xe is well established.[9,10] Our findings suggest that, in the case of the X/RGS charge-transfer states, the equivalent transition occurs in going from Xe to Kr.

 0021-9606/90/084856-20$03.00

In contrast with X/Rg single host solids, in X/Rg/Rg' mixed hosts, delocalization effects can be completely absent. Examples that are well documented are solid F/Xe/Ar and F/Xe/Ne, in which the diatomic Xe^+F^- charge transfer states maintain their localized, molecular integrity.[11–15] Although somewhat perturbed, both excitation and emission spectra in these systems can be directly related to the gas-phase diatomic XeF potentials. Moreover, these matrix-isolated exciplexes retain most of their gas-phase molecular characteristics, including their lasing properties.[14,15] In this paper we show that, even in the absence of extensive delocalization, not all diatomic exciplexes can be isolated in such ternary solids. In F/Kr/Ar, while the excitation resonances correspond to the isolated diatomic Kr^+F^- exciplex, the emission is strictly from the mixed triatomic exciplex, $(ArKr)^+F^-$. This finding, in itself, is not too surprising, since the latter is also a well-known stable gas-phase species.[16] This system, however, enables the establishment of time scales for the interconversion between the diatomic and triatomic configurations; a process equivalent to excitonic self-trapping by lattice relaxation.[17–19]

Given the extensive gas-phase data on both ionic and covalent rare-gas–halogen interactions, it is possible to scrutinize the solid-state spectra to provide a useful description of the potential surfaces that govern molecular dynamics in these systems. As such, we provide analyses of both the continuum emission spectra and the discrete excitation spectrum in F/Kr/Ar. The latter is used, together with molecular-dynamics simulations, to extract information on the trapping sites and motions of F atoms on the ground surface. This also serves as the basis for commenting on the adequacy of gas-phase pair potentials in describing energetics in the crystalline solids.

In addition to charge-transfer states of the atomic X/RGS systems, those of the molecular halogens, X_2/RGS, are of significant interest. The reactive dynamics that follows the photo-induced charge transfer between the rare gas and a molecular halogen—in solid, liquid, and gas phase—has been extensively discussed under descriptive headings, such as photoinduced harpooning.[20] In the case of solid-state studies, two aspects of these processes are noteworthy: (a) they lead to very efficient dissociation of products out of the solid cage,[21] and (b) the two-photon induced transitions,

$$X_2Rg + 2h\nu \rightarrow [Rg^+X_2^-] \rightarrow Rg^+X^- + X, \qquad (1)$$

are characterized by inordinately large cross sections.[1,2,20] The absorption process in (1) is an example of a cooperative transition, which is particularly efficient in condensed media.[22] The experimental demonstration of the coherent nature of these transitions in the case of molecular halogens has been difficult in the past, due to possible interferences from sequential two-photon channels.[23] Given the simplicity of its electronic potentials in the UV-VIS spectral range,[24] molecular F_2 is particularly well suited for the characterization of this process. As such, we have measured both, the two-photon absorption cross section and two-photon photodissociation cross section in F_2/Kr, and verified the absence of sequential two-photon excitation channels. The very large absorption cross sections of these transitions are rationalized in the framework of "giant two-photon absorption" theories developed for the treatment of excitonic molecules.[25] Finally, a comparison of photodissociation cross sections via the traditional one-photon dissociation and via the two-photon induced harpoon process for F_2 in solid Kr is possible, and will be reported.

The molecular exciplexes, once formed, relax via radiative bound-to-repulsive transitions. In the gas phase, such a transition would lead to the impulsive separation of the neutral atoms. Hence, the nomenclature of "radiative dissociation," which is used in referring to this process. In solids, the same transition leads to the sudden creation of hot atoms, 0.5–1 eV above ground. The modes of dissipation of this excess energy, and the fate of the hot atoms produced in the solid, are an important part of the photocycle in these systems, which hitherto has received little attention. The dynamics of this process is quite analogous to that of photodissociation, a main difference being the excitation mode: in radiative dissociation, well-defined cage coordinates are directly excited; while in photodissociation, only guest modes are excited by the radiation. Issues, such as cage exit and subsequent migration of guest atoms, are common to both investigations, and the complimentary information provided by the two approaches should lead to a deeper understanding of reactive dynamics in condensed matter. The final dissipation step in all reactive dynamics in solids is the degradation of the locally released excess energy into the phonon bath. Radiative dissociation studies are well suited for detailed investigations of this final relaxation step. Experimental observations of both the launching and subsequent thermalization of acoustic displacement waves, and reversible and irreversible creation of defects, upon the radiative dissociation of Kr_2F in polycrystalline Kr will be described. Direct experimental observations of mass transport accompanying the same process are also presented. The latter is accomplished in solid Ar multiply doped with Xe, Kr, and F, in which the F atoms are shown to reversibly shuttle between Kr and Xe sites by the optical excitation. Detailed theoretical[26] and experimental[27] studies of the complimentary processes, direct photodissociation of F_2 and subsequent migration of F atoms in RGS, will be reported in subsequent papers.

II. EXPERIMENT

The experiments to be reported here were conducted in several different types of solids. Conventional matrix isolation techniques were used in some, and free-standing crystals were used in most of the investigations. The different types of solids represent different experimental conveniences; however, most of the results to be reported are independent of the type of solid used. The techniques and apparatus used for the crystal growth are similar to those used by Rudnick *et al.*[28] with only minor modifications. A rectangular glass tube of 1 cm × 1 cm profile is used as a mold for the crystal. The rectangular tube is fused to a 1/4 in. glass tubulation, which is fed through a double "O"-ring connection on the cryostat vacuum shroud. The glass mold is brought in contact with the cryotip of either a closed-cycle refrigerator (Air Products Displex, DE-202), or a He flow cryostat (Air

Products, Heli-tran) at the beginning of the growth, and retracted manually at the end. The premixed gas at a pressure of ~250 Torr is maintained throughout the growth either by an on-line pressure regulator, or by an adjustable leak valve. Crystals of ~1 cm^3 volume are grown within ~20 min. As long as the dopant concentrations are kept low, the resulting crystals are optically clear. A gold-Chromel thermocouple, embedded in the crystal during its growth, is used for temperature measurements. In this method of preparation, the solid grows across a large thermal gradient. Therefore, clustering and segregation of impurities are potential problems that should be characterized in a given experiment. Recent infrared (IR) studies of these solids indicate that in commensurate guest hosts, and in particular for impurities lacking permanent dipoles, nearly perfect isolation is possible, while in other cases the impurities tend to segregate.[29] In the case of F_2-doped solid Ar and Kr, and for dilutions in excess of 1:1000, no concentration gradients or any evidence for clustering could be observed. We therefore assume that the F_2 molecules are well isolated in substitutional sites of the crystalline solids. This assumption has been amply verified in recent molecular-dynamical simulations, which indicate that F_2 fits loosely in substitutional sites of solid Ar and Kr.[26]

Either multigas excimer lasers, or excimer pumped dye lasers, are used as excitation sources. Emission at 90° from the excitation source is collected by a variety of optical arrangements—a 1/4 m monochromator fitted with a photomultiplier (PMT), or a 1/4 m polychromator fitted with an intensified diode array are used most commonly. Spectral calibration is provided by a Hg penlight. The experimental design in the detection of acoustic waves is illustrated in Fig. 1. An excimer laser is used as the excitation source and an excimer pumped dye laser is used as the probe. The excimer is focused through a cylindrical lens in the vertical direction, while a horizontally propagating dye laser is made to overlap the excitation plane. Several detection geometries are used for the exiting dye beam. In the simplest of geometries, the dye laser spot is made larger (0.5 mm) than the pump waist (0.1 mm), and different portions of the dye beam are selected with an iris. Alternatively, the dye laser is monitored through a fixed iris and the excimer beam waist is laterally displaced by a micrometer. In several studies, the transmitted probe beam was expanded with a negative lens, and subsequently line focused with a cylinder lens on the detection plane. This arrangement provided a magnification of 50 and enabled accurate determinations of the displacement between pump and probe volumes, with a resolution of ~10 μm. The timing of the two lasers is controlled via a digital delay generator. The transmitted beam is detected by a fast-diode, and captured with a digital storage scope (Tektronix 2440) operating in the envelop mode. The scope is triggered from a diode monitoring the excimer beam. The technique completely eliminates time jitter between the two lasers. However, since no averaging is used, the signal-to-noise ratio is limited by the intensity jitter of the laser outputs to ~20:1. Thus, in the present setup, transients that lead to gain or loss in excess of ~5% can only be observed.

High-purity gases, F_2(97%), Ar(99.999%), Kr(99.999%), are used in these studies. Except for argon, which was passed through a cold trap held at liquid-nitrogen temperature before using, all gases were used with their original purities. The precaution in the case of Ar was necessary in order to eliminate its Xe content, which appeared to be the major impurity in the sample. All sample manipulations were conducted in a greaseless, glass vacuum manifold, fitted with Teflon seated stopcocks.

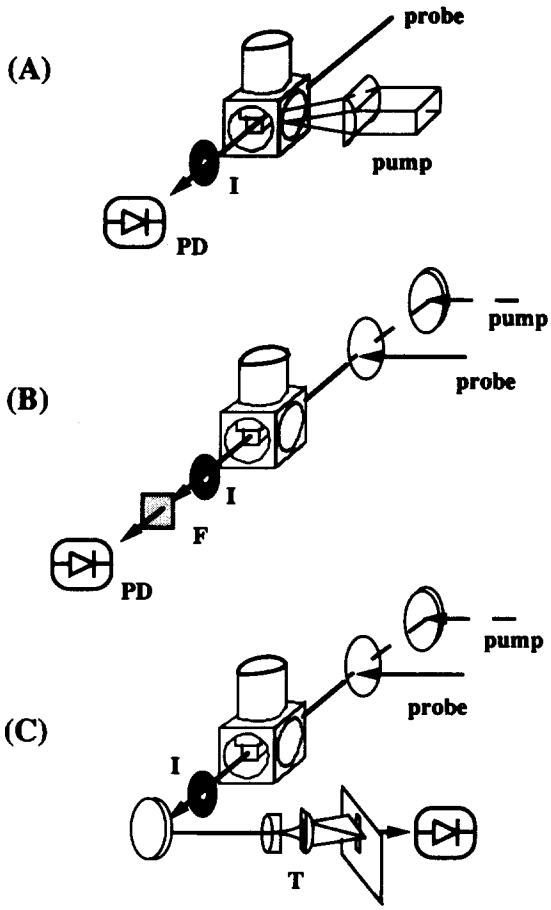

FIG. 1. Experimental arrangements for pump-probe studies. (I = iris, PD = photodiode, F = filter, T = telescope.) (A) Transverse pumping: An excimer laser operating at 248 nm is used as the pump source, and an excimer-pumped dye laser as the probe. The transmitted probe beam is spatially filtered and detected with a fast photodiode. (B) Longitudinal pumping: A doubled dye laser operating at 275 nm is used as pump source. The pump and probe are overlapped through a beam splitter. The UV beam is blocked by an optical filter. (C) Longitudinal pumping with magnification of the transmitted probe beam: Magnification is provided by the combination of a negative lens and a cylindrical lens. The line image is then detected through a 0.5 mm slit. The arrangement provides a magnification of 50, enabling spatial resolution in the pump volume of 10 μm. The time delay between pump and probe is controlled and scanned by a digital delay generator. The photodiode signal is recorded by a digital oscilloscope operating in envelope mode.

III. RESULTS

A. Spectroscopy of KrF/Ar

Excitation and emission spectra from an F:Kr/Ar free-standing crystal are shown in Figs. 2(a) and 2(b), respec-

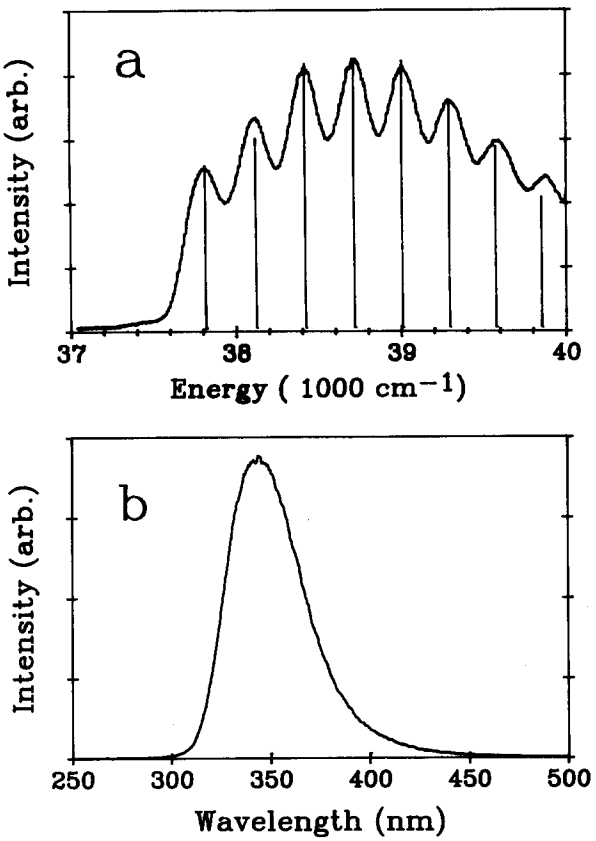

FIG. 2. (a) Laser excitation spectrum of the $(ArKr)^+F^-$ emission at 343 nm in a 1:1:1600 F_2:Kr:Ar crystal at 12 K. The vertical sticks are the simulated intensities with the assumption of a Gaussian ground state and distance-dependent transition dipole. (b) Emission spectrum of $(ArKr)^+F^-$ with 260 nm excitation. The spectrum was obtained after extensive irradiation of a 1:1:1600 F_2:Kr:Ar crystal with 308 nm light and was recorded with an optical multichannel analyzer (OMAIII).

tively. The solid was prepared from a gas mixture of F_2:Kr:Ar of 1:1:1600, and extensively irradiated at 308 nm to complete the dissociation of the molecular fluorine. The emission spectrum was recorded with 260 nm excitation. This broad emission, which peaks at 343 nm, is the only emission observed for excitation wavelengths between 230 and 280 nm. It is assigned to the triatomic $(KrAr)^+F^-$. In solid Ar, the fluorescence decays exponentially with a lifetime of 60 ± 5 ns. The insensitivity of the fluorescence lifetime to preparation conditions, and to temperature of the solid, leads us to believe that it represents the radiative lifetime of the vibrationally relaxed exciplex, as in all previously studied solid-state triatomic exciplexes.[2,20]

The excitation spectrum shown in Fig. 2(a) was recorded by scanning a frequency-doubled, excimer-pumped dye laser, while monitoring the triatomic emission shown in Fig. 2(b). The excitation spectrum clearly shows the diatomic vibrational progression of KrF(B). This spectrum has previously been observed and assigned in rare-gas matrices.[11,12] A detailed analysis of the spectrum will be presented in Sec. IV. We note that the vibronic excitation line shapes are rather broad and symmetric—atypical of excitation line shapes for stable matrix-isolated species. A characteristic of the latter would be the observation of a zero-phonon line accompanied by phonon sidebands. It will be argued in Sec. IV that these linewidths are controlled by lifetime broadening—the interconversion time of the diatomic to the mixed triatomic configuration.

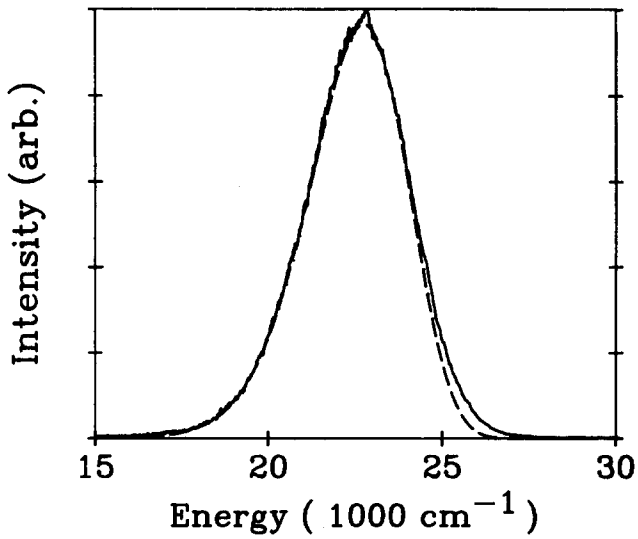

FIG. 3. Emission spectrum of $(Kr_2)^+F^-$ with 248 nm excitation in crystalline krypton at 12 K. F_2:Kr = 1:3000. The dashed line displays the simulated band profile obtained using the reflection approximation for the $Kr_2^+ \rightarrow Kr_2$ vertical neutralization process (see text).

B. Spectroscopy of F/Kr

F-doped Kr solids, both matrices and free-standing crystals, are prepared by photodissociation of samples originally doped with F_2. Near-UV excitation of such solids produces emission from $Kr_2^+F^-$. An emission spectrum from a crystalline sample is shown in Fig. 3. The emission

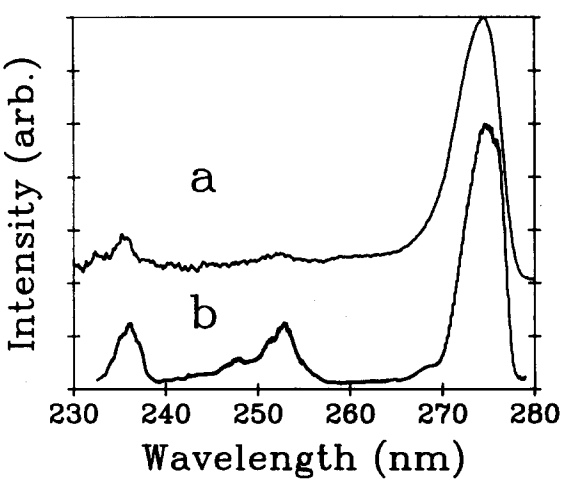

FIG. 4. Excitation spectrum of the $(Kr_2)^+F^-$ emission at 453 nm in solid krypton at 12 K. (a) Spectrum was recorded using monochromatized Xe arc illumination of a matrix with original sample composition F_2:Kr = 1:3000. (b) Spectrum from a free-standing crystal of F_2:Kr = 1:3000. Excitation source is a frequency-doubled dye laser.

peaks at 453 nm possess a full width at half maximum (FWHM) of 63 nm and have a fluorescence lifetime of 140 ± 10 ns.

Excitation spectra recorded while monitoring the triatomic emission are illustrated in Fig. 4. Spectrum a is from a thin matrix, and was recorded using the monochromatized output of a 75 W Xe arc lamp. A 1/4 m monochromator, with slit equivalents of 1 nm bandpass, was used for this purpose. The spectrum was obtained after background subtraction and ratioing with the intensity profile of the lamp output. The main excitation feature is centered at 274.5 nm. Weaker features can be observed near 253 and 236 nm. Annealing of F-doped matrices is not possible, since as the temperature of the solid is increased above ~17 K the F atoms diffuse and recombine on the time scale of several minutes. Spectrum a was obtained after several irradiation and warmup cycles of the matrix. Spectrum b in Fig. 4 was obtained from an extensively irradiated free-standing crystal, using the doubled output of an excimer-pumped dye laser. The major aim of this study was to unravel any resolvable structure underneath the main excitation band at 275 nm. As can be seen in Fig. 4, the laser and lamp spectra are nearly identical (the slight rounding of the peak in the crystal spectrum is due to the large outer diameter of the 1 cm long crystal at the absorption maximum). Quite clearly, this band does not have any resolvable structure. The higher-energy peaks are more prominent in the spectrum obtained in the crystal. The relative intensity of these bands is strongly dependent on sample preparation, history, and temperature.

C. Photogeneration of F atoms in Kr

Photogeneration of F atoms from F_2-doped Kr crystals is possible by two very distinct mechanisms: (a) photodissociation via the molecular $^1\Pi_u$ repulsive surface and (b) two-photon-induced harpooning. The first of these processes can be followed by two color experiments in which one photon is used to dissociate the molecule, and a second is used to monitor the F-atom concentration via the Kr_2F emission. A 308 nm laser is used as the dissociation source, and a frequency-doubled dye laser, operating at 275 nm, is used as the F-atom probe. Care is taken to maintain the probe intensity (~10 nJ/pulse) 5–6 orders of magnitude weaker than the photodissociation beam intensity, in order to avoid significant photodissociation by the 275 nm pulse. Such a measurement would yield the concentration of permanently dissociated F atoms. If there were any recombination of the time scale of delay between dissociation and probe, then effectively a lower photodissociation quantum yield would be obtained. In order to gauge the extent of such recombination, for every 308 nm pulse, two 275 nm probe pulses, at two different delays from the dissociation pulse, are used: one, delayed by 100 ns, and a second, delayed by 50 ms. The emission intensity under each probe pulse is then separately averaged with independent boxcars. Exponential growth of the F-atom concentration is observed, and the growth curves obtained with the two different delays were always identical. An example of such a growth, taken from a free-standing crystal of F_2:Kr, 1:7000, is shown in Fig. 5(a). Given the very weak F_2 absorption at 308 nm,[30] $\sigma = 2.1 \times 10^{-20}$ cm^2, the sample remains optically thin throughout the measurement. From the exponential fit to the growth curve, a photodissociation cross section $\gamma = 1 \times 10^{-20}$ cm^2 is obtained (growth in emission intensity, E, given as $E(t) = E_\infty [1 - \exp(-\gamma I t)]$). Using the gas-phase absorption coefficient of F_2 at 308 nm, this photodissociation cross section would imply a dissociation quantum yield $\phi = \gamma/\sigma = 0.5$.

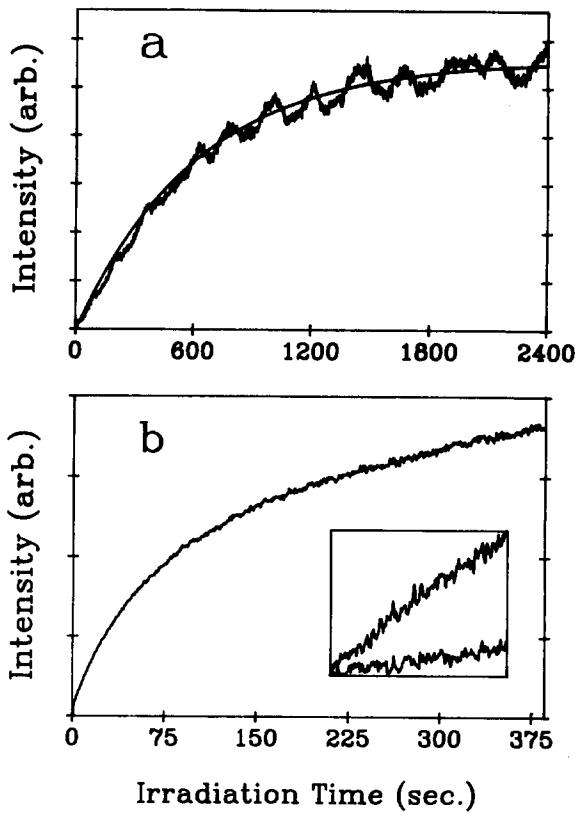

FIG. 5. (a) Growth of the $(Kr_2)^+F^-$ emission at 453 nm in a 1:7000 F_2:Kr crystal as a function of irradiation time with 308 nm laser light. Laser fluency is 9.5 mJ/cm^2 (10 Hz repetition rate). The emission was induced by a weak probe at 275 nm delayed by 100 ns from the 308 nm dissociation pulse. (The fluctuations are due to the time jitter in the laser pulse under the narrow boxcar gate.) (b) Growth of the 453 nm emission in a 1:20 000 F_2:Kr crystal while irradiated at 275 nm (41 mJ/cm^2, 20 Hz repetition rate). Inset shows the early growth at two different powers. The slopes of the early growth rates show a power dependence of 2($\pm$0.02).

When F_2/Kr samples are irradiated near the F/Kr excitation maximum, a two-photon-induced growth of the Kr_2F emission is observed. An example of the emission growth for an F_2:Kr, 1:20 000 sample while irradiated at 275 nm is presented in Fig. 5(b). The growth is clearly nonexponential. A test of the power dependence of the early time growth (illustrated in the inset to the figure) indicates that the growth rate quadruples when the irradiation fluence is doubled. The shape of the growth is characteristic of two-photon-induced harpooning with the generation of a strongly absorbing product.[1,2] Near 275 nm, due to the very strong absorption by F/Kr (see excitation spectrum in Fig. 4), even at a dilution of 1:20 000 the crystal cannot be maintained optically thin. Exact analysis of such growth kinetics requires integration of the pertinent rate expressions in both time and space,

since the radiation field decays as it traverses the solid (for details see Refs. 1 and 2). Moreover, given the large dimensions of the solid used in the present studies, exact definition of the volume from which the fluorescence is collected is essential in quantitative treatments. Here, we are only interested in order-of-magnitude estimates of the two-photon dissociation cross section. As such, using the growth half-life, and the measured excitation fluence (2 MW cm^{-2}), a cross section of $3(\pm 2)\times 10^{-45}$ cm^4 s is obtained. This estimate represents a lower limit to the true cross section since absorption and scattering losses of the laser are neglected. Finally, we note that what is being measured here is the two-photon-induced permanent dissociation cross section of F_2 in Kr. If upon two-photon excitation, the dissociation quantum yield is not unity, then the excitation cross section is even larger than this estimate.

A direct measure of the two-photon absorption cross section is afforded by monitoring the transmission with time of a tightly focused 275 nm beam on a virgin F_2/Kr sample. Since the molecular fluorine absorption cross section is of order 10^{-20} cm^2 at 275 nm,[30] for fluences in excess of 10^{25} cm^{-2} s^{-1} the two-photon absorption is dominant originally. However, upon photogeneration of the F atoms, the one-photon charge-transfer absorption cross section of F/Kr can become significant. In a 1:7000 F/Kr sample, transmission measurements were conducted as a function of excitation fluence. At high fluences, a net increase in transmission with irradiation time is observed—50% increase, for a fluence of 3.5×10^{26} cm^{-2} s^{-1}; while at low fluences a net loss is observed—85% for fluences less than 1×10^{24} cm^{-2} s^{-1}. The low-intensity measurements yield the absorption cross section of F/Kr—3.9×10^{-19} cm^2 at 275 nm. When taken into account, a two-photon absorption cross section of $2.8(\pm 2)\times 10^{-45}$ cm^4 s can be extracted from the high-intensity measurements. The largest source of error in the latter figure is the estimate of the spot size of the focused laser beam in the sample. A comparison of the two-photon absorption cross section with the two-photon-induced photodissociation cross section discussed above indicates that within the experimental errors of $\sim 50\%$ the dissociation quantum yield via the two-photon process is unity.

While clearly a two-photon-induced charge transfer and dissociation are being observed, the possibility that the process is due to a sequential absorption remains. Such a scheme could, in principle, be expected if the $F_2(^3\Pi_u)$ surface was stabilized by the cage to sustain population long enough to be reexcited. The triplet surface would then be expected to be populated during the geminate recombination of the F atoms, after the dissociative excitation to the $^1\Pi_u$ surface. The second photon would then induce the charge transfer from Kr to $F_2(^3\Pi_u)$ at much longer wavelengths than $F_2(X)$ due to the ~ 2 eV increase in vertical electron affinity of the excited state. This mechanism has recently been demonstrated for Br_2 in liquid xenon, in which the deeply bound A/A' states act as a reservoir for the recombinant atoms.[23] Two-color experiments, designed to test this hypothesis, failed to show any contribution from such a sequential excitation channel. In these experiments, a 308 nm laser was used as the $^1\Pi_u \leftarrow X$ excitation source, and a 275 nm laser was used to effect the charge transfer. The exciplex emission intensity was independent of the order of precedence of the two pulses, and no enhancement could be seen when the two pulses were coincident in time. Contributions from sequential two-photon processes are clearly negligible in the present case. A second conclusion to be made is that geminate recombination due to the cage proceeds predominantly via the ground surface.

D. Pump-probe studies

The setup for pump-probe studies was described in the experimental section. Several variants of the geometry were used with two main aims in mind: (a) the modes of kinetic-energy accommodation by the lattice, upon radiative dissociation of the exciplex, and (b) a search for transient optical gain, or loss, in these potential laser media. Free-standing crystals of F/Kr were used for these studies. In the transverse geometry, a gas-phase KrF laser operating at 248 nm was tightly line focused in the center of the crystal with a cylindrical lens (focal length of 4 in.). The resulting beam waist was estimated to be ~ 100 μm. An excimer pumped dye laser, operating at 465 nm, was used as a probe. In probing the pumped volume, the dye laser traveled the 1 cm length of the crystal at 90° to the pump beam and coplanar with it. When the transmitted dye beam from the overlap

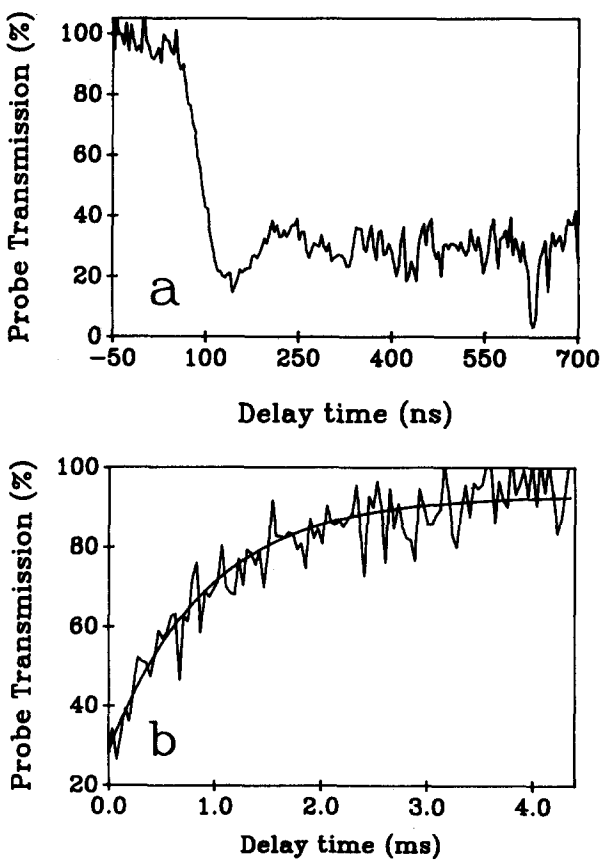

FIG. 6. Transient loss in a 1:3000 F_2:Kr crystal as a function of delay between pump and probe lasers. Transverse pumping geometry is used with $\lambda_{pump} = 248$ nm (300 MW/cm^2) and $\lambda_{probe} = 465$ nm. (a) displays the onset of the main loss and (b) shows the ms time-scale recovery.

region is detected, a strong transient loss is observed, as shown in Fig. 6(a). The onset of the main loss is delayed relative to the pump edge by ~ 150 ns, namely the radiative lifetime of Kr_2F. The recovery of the probe beam occurs exponentially on a time scale determined by the pump intensity. In the example shown in Fig. 6(b), the pump fluence was 300 MW cm^{-2}, and the recovery time is ~ 2 ms. In this example, while the transient loss is $\sim 80\%$, the recovery is complete between pump pulses. At higher fluences, permanent damage of the solid is observed—the probe transmission does not return to base line, and this permanent scattering loss accumulates with repeated pumping. When the pump and probe volumes are displaced (either by translation of the pump beam relative to the probe, or by translation of the iris on the exit side of the probe beam), the onset of the transient loss is further delayed. Examples are provided in Figs. 7(a) and 7(b). Finally, when a collection lens replaces the exit iris, within experimental error of $\sim 5\%$, neither loss nor gain is observed. In a final study, the transmitted probe beam was magnified by 50:1 and line focused on the detector plane. Translation of the photodiode along the magnified linear image of the probe volume showed transient loss near the center of the probe volume and transient gain at the edges. These tests serve to establish scattering of the probe beam as the main source of the observed transient loss.

The delay in the loss onset, even for the case when the pump and the probe are perfectly overlapped, is a clear indication that the main loss is not due to a transient absorption by the excited state. The observation of delayed transient loss outside the pump volume is a clear indication that at least the onset is due to light scattering, due to acoustic displacement waves created by the kinetic energy released upon the radiative dissociation of the exciplex. The group velocity of the wave can be obtained from the knowledge of the displacement between pump and probe beams, and from the observed delay in the loss onset. Such measurements yielded values of $1.75(\pm 0.5)\times 10^5$ cm s^{-1} and $2.5(\pm 0.5)\times 10^5$ cm s^{-1} for the group velocities measured by the different methods. Previous direct measurements yielded a value of 1.38×10^5 cm s^{-1} for the velocity of longitudinal sound waves in polycrystalline Kr.[31] Given the errors inherent in our measurements, these values should be taken to be in agreement, enabling the identification of the scattering mechanism as due to acoustic deformation waves. The long-time recovery of the loss, under intense pumping conditions, however, just below the threshold for permanent damage, can then be attributed to the creation of defects on the scale of the wavelength of the probe beam and their subsequent annealing. The extreme pumping conditions used in these preliminary studies were necessary given the weak absorption of the solid at 248 nm, and the requirement of a signal-to-noise level above the combined intensity jitter of the two lasers of $\sim 10\%$. It should be noted that at 248 nm, two-photon access of the Kr excitonic absorption is possible, and undoubtedly contributes to the observed dynamics. In order to eliminate such contributions, and to operate at much lower pump fluences, we carried out a set of measurements in the longitudinal pumping geometry, using a pump laser resonant with the KrF absorption at 275 nm.

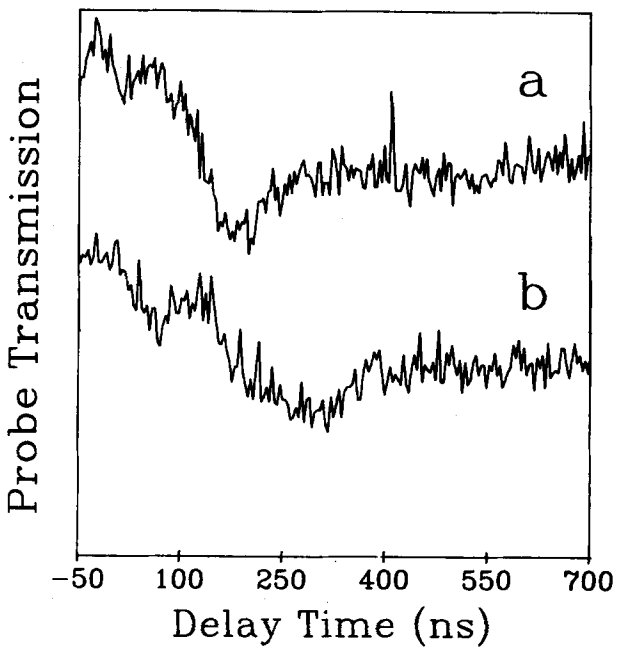

FIG. 7. The onset of the transient loss in a F_2:Kr crystal. (a) Pump and probe volumes are perfectly overlapped. (b) Probe volume is displaced by 200 μm with respect to the pump. For experimental conditions see Fig. 6.

In the longitudinal pumping geometry, a doubled dye laser operating at 275 nm was spatially overlapped with the probe laser through a 100 μm thick sapphire beam splitter. The collinear beams were then focused with a single lens on the crystal. The main observations of the transverse pumping geometry could be repeated with this setup. Additionally, several new observations could be made. Under mild pumping conditions, both purely ballistic and diffusive acoustic waves could be observed. The first is characterized by a sharp scattering loss peak [Fig. 8(a)], while the second is characterized by a sharp rise followed by a tail that decays on a sub-microsecond time scale [Figs. 8(b) and 8(d)]. The creation of defects and reversible annealing characterized by exponential recovery on the time scale of 10^{-4} s could also be observed [see Fig. 8(c)].

In the longitudinal pump-probe experiments, in addition to the delayed loss, a small loss peak which recovers on the time scale of ~ 100 ns can be observed at zero delay [see Fig. 8(d)]. Given the fact that this loss peak occurs at zero delay, it is tempting to assign it to an optical absorption, i.e., to transient absorption by the triatomic exciplex. With this assumption, and using a cross section of 3.9×10^{-19} cm^2 for the absorption of F/Kr at 275 nm (which was determined above), and under the assumption that the triatomic exciplex is formed with unit quantum efficiency, at 440 nm, a cross section of 1.4×10^{-18} cm^2 is deduced for the net loss due to the solid-state absorption of Kr_2F. These measurements were repeated at discrete wavelengths between 435 and 475 nm. At all studied wavelengths, a structureless transient absorption of similar cross section was observed. Several observations lead us to question this interpretation: (a) when a collection lens is used on the transmitted beam, no loss can be observed, (b) under certain conditions of align-

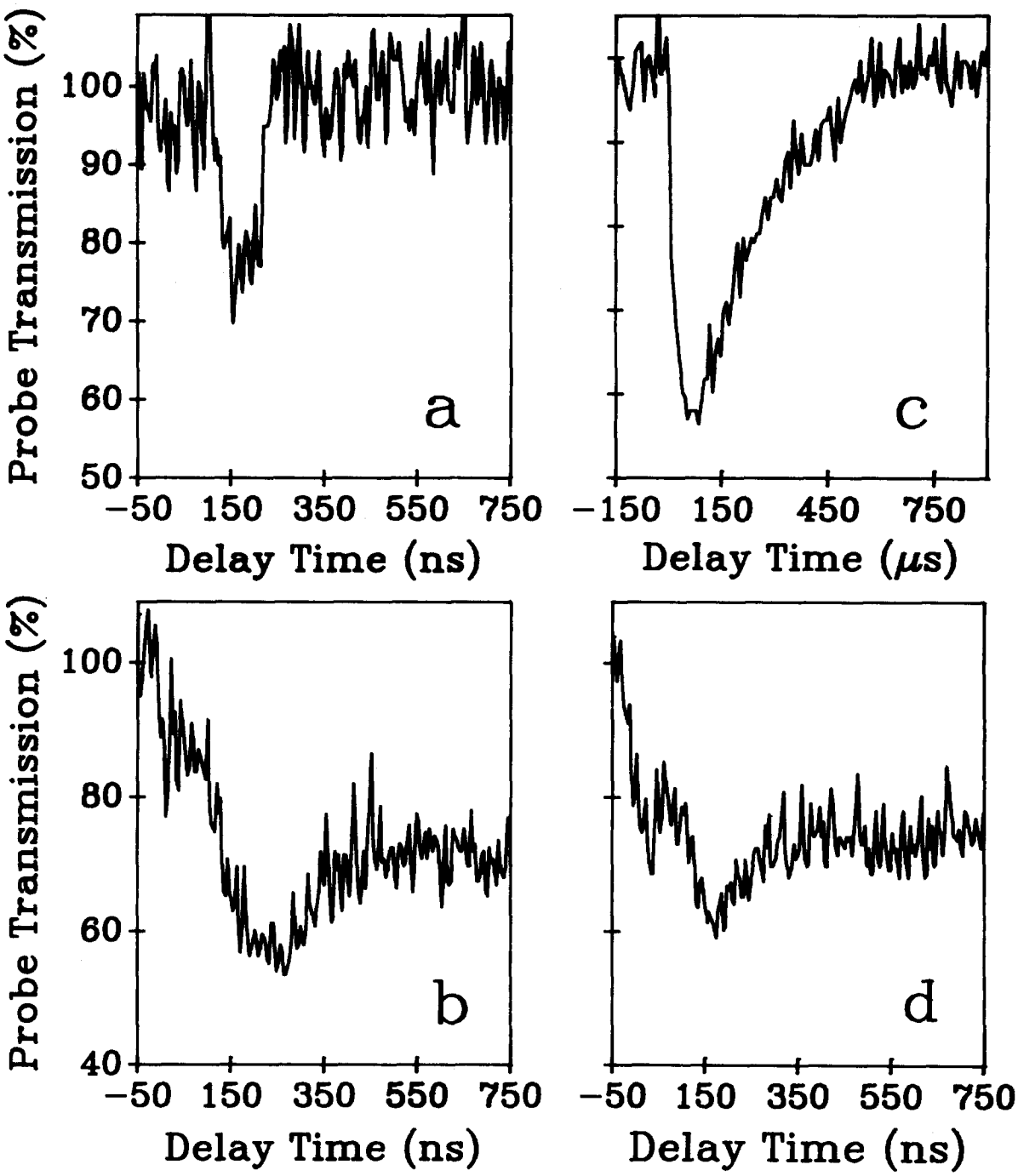

FIG. 8. Transient loss in a 1:3000 F_2:Kr crystal as a function of delay between pump and probe laser pulses. Longitudinal pumping geometry is used with $\lambda_{pump} = 275$ nm (2.7 MW/cm^2) and $\lambda_{probe} = 450$ nm. (a) Ballistic acoustic wave. (b) Diffusive acoustic wave. (c) μs recovery of the loss (note the different time scale). (d) Transient absorption at zero delay.

ment the initial loss peak is delayed, (c) in several scans, in addition to the prompt loss a 5% gain is observed prior to the main loss peak. These observations would argue that the nature of the prompt loss is also due to scattering as opposed to absorption. The kinetic energy of $\sim$0.5 eV released during the formation of the triatomic exciplex, which proceeds on a subpicosecond time scale, could be responsible for this initial scattering loss.

E. F:Kr:Xe/Ar solids

Multiply doped free-standing crystals are used to investigate the mobility of atoms upon the radiative dissociation of the different exciplexes. In the experiments to be reported, the samples were prepared from an F_2:Kr:Ar gas mix of 1:1:3800; however, the Ar was not diluted in order to introduce trace amounts of Xe. According to the manufacturer's

specifications the Xe content should be of order 1 ppm. In Fig. 9 emission spectra obtained from this experiment are presented in chronological order in panels (a) through (f). All spectra are recorded with 248 nm excitation. However, the excitation geometry and volume are changed among the different spectra, and therefore the absolute emission intensities should not be compared to each other. All of the presented spectra are single-shot records obtained with the optical multichannel analyzer (OMA).

After irradiation of the sample by several pulses at 248 nm (24 mJ cm^{-2}), the spectrum in Fig. 9(a) is obtained. The two emissions can be identified as the narrow XeF($D \rightarrow X$) band at 286 nm, which relaxes on a time scale shorter than the pump pulse width, and the broad $(ArKr)^+F^-$ emission at 343 nm, with a radiative lifetime of 60 ns. The growth of these emissions was followed in real time. Over a period of 100 min irradiation at 248 nm (4 Hz, 24 mJ cm^{-2}), the growth in both emissions was observed to be linear, i.e., followed zero-order kinetics, with the XeF growth rate nearly twice that of ArKrF. The spectrum in Fig. 9(b) was obtained after this extensive irradiation period, and clearly shows the differential growth—the relative heights of the emission peaks are reversed between Figs. 9(a) and 9(b).

The same volume of the crystal was subsequently irradiated at 308 nm for a period of 45 min, at 20 Hz, and 7 mJ cm^{-2} pulse. The spectrum in Fig. 9(c) was recorded by 248 nm excitation immediately after this irradiation period. More than a tenfold increase in the ArKrF emission occurs during 308 nm excitation, while the XeF emission subsides by a similar factor.

The sample was subsequently irradiated at 248 nm for a period of 30 min, 4 Hz, 24 mJ cm^{-2} and the spectrum in Fig. 9(d) was recorded. The cycle clearly repeats itself, as in the first 248 nm irradiation period the XeF emission intensity grows, while the ArKrF emission subsides.

The spectrum in Fig. 9(e) was obtained after 30 min irradiation at 308 nm, using a 6 in. lens to generate high fluency, $\sim$70 mJ cm^{-2}. Transverse pumping was subsequently used for the 248 nm excitation, using a cylinder lens with the resultant intensity at the beam waist estimated as 700 mJ cm^{-2}. As in the previous 308 nm irradiation cycle, the XeF emission subsides while the ArKrF emission grows. In addition, the Kr_2F emission band at 439 nm, with a lifetime of 140 ns, appears.

The spectrum in Fig. 9(f) was obtained after warm-up of the sample to 30 K and cooling back to 12 K. The only emissions observed are those of XeF—the $D \rightarrow X$ band at 286 nm, and the $D \rightarrow A$ band at 340 nm; both ArKrF and Kr_2F emissions effectively disappear by the heat cycle.

IV. DISCUSSION

A. F:Kr/Ar

The typical emissions that may be expected from a diatomic exciplex when excited to the B state would be a narrow $B \rightarrow X$ band and a broad $C \rightarrow A$ band. An example of this situation in the published literature is that of XeF isolated in solid Ar.[11–14] If the C state is below B, and an efficient intersystem crossing occurs between these two electronic states, then a narrow $C \rightarrow X$ and a broad $C \rightarrow A$ band are to be expected. An example of this case is that of XeCl in Ar and Kr matrices.[1] Furthermore, the emission wavelengths of diatomic exciplexes in rare-gas solids can usually be well predicted based on the known gas-phase emissions, after taking into account the dielectric shift due to the medium. The absence of such emissions, and the observation of only a broadband peaking at 343 nm when the KrF(B) state is accessed optically (see Fig. 2), leads us to assign the emission to the mixed triatomic exciplex, namely, $(ArKr)^+F^-$. In the gas phase, this emission peaks at 305 nm.[16] A shift in emission due mostly to solvation of the exciplex dipole in polarizable media is to be expected. The observed bandwidth of FWHM = 2000 cm^{-1} is typical for solid-state triatomic exciplexes, and the lifetime of 60 ns, while somewhat shorter than that of the symmetric triatomics [$\tau(Kr_2F) = 140$ ns in solid Kr, $\tau(Xe_2F) = 190$ ns in solid Xe (Ref. 2)], it is in a range that can be rationalized based on the asymmetry of the ionic state—the lifetime is intermediate between the diatomic and triatomic exciplexes. In contrast with the present results, the only emission reported by Ault and Andrews in their mixed F_2:K:Ar, 1:1:100 matrices was a broadband at 435 nm.[11] This is closer to the emission peak of Kr_2F at 453 nm observed in F:Kr solids, and in better agreement with the Kr_2F emission at 439 nm observed in solid Ar [see Fig. 9(e)]. Given the concentrations used in their experiments, the photogenerated F atoms will be formed in sites containing more than one Kr (see below), and hence the main emission in those studies should probably be assigned to $Kr_2^+F^-$ isolated in Ar.

The observation of diatomic resonances in the excitation spectrum, and only the triatomic in emission, implies a very efficient interconversion between these two molecular charge-transfer configurations. This interconversion time scale can be bracketed between 20 and 500 fs. The lower limit is determined by the symmetric, vibronic excitation linewidths of FWHM = 265 cm^{-1}. The upper limit can be obtained from the consideration that $B \rightarrow X$ contributions to the emission are completely absent. Based on the signal-to-noise ratio of the spectrum in Fig. 2(b), it can be concluded that the quantum yield of emission from the B state is less than 10^{-4}. Using the gas-phase radiative lifetime of the B state of 9 ns,[32] a lifetime of 5 ns is to be expected in Ar[33] which places an upper bound of 500 fs on the lifetime of the diatomic B state in Ar. Thus, an efficient charge rearrangement leads to the formation of the triatomic exciplex. The observation of Kr_2F emissions in concentrated F:Kr/Ar solids implies that the charge rearrangement in sites where F atoms are surrounded by more than one Kr leads to the formation of the more stable symmetric triatomic configuration on the same fast time scale.

Analysis of the excitation spectrum of Fig. 2(a) is straightforward. Based on the sharp onset on the red edge, the first line in the progression can confidently be assigned to the 0–0 transition of KrF($B \leftarrow X$). With this assignment, a least-squares fit to the vibrational spacings yields the harmonic frequency, anharmonicity, and electronic origin of the transition. These parameters are collected in Table I, along with those of the gas phase[34,35] and the previous matrix

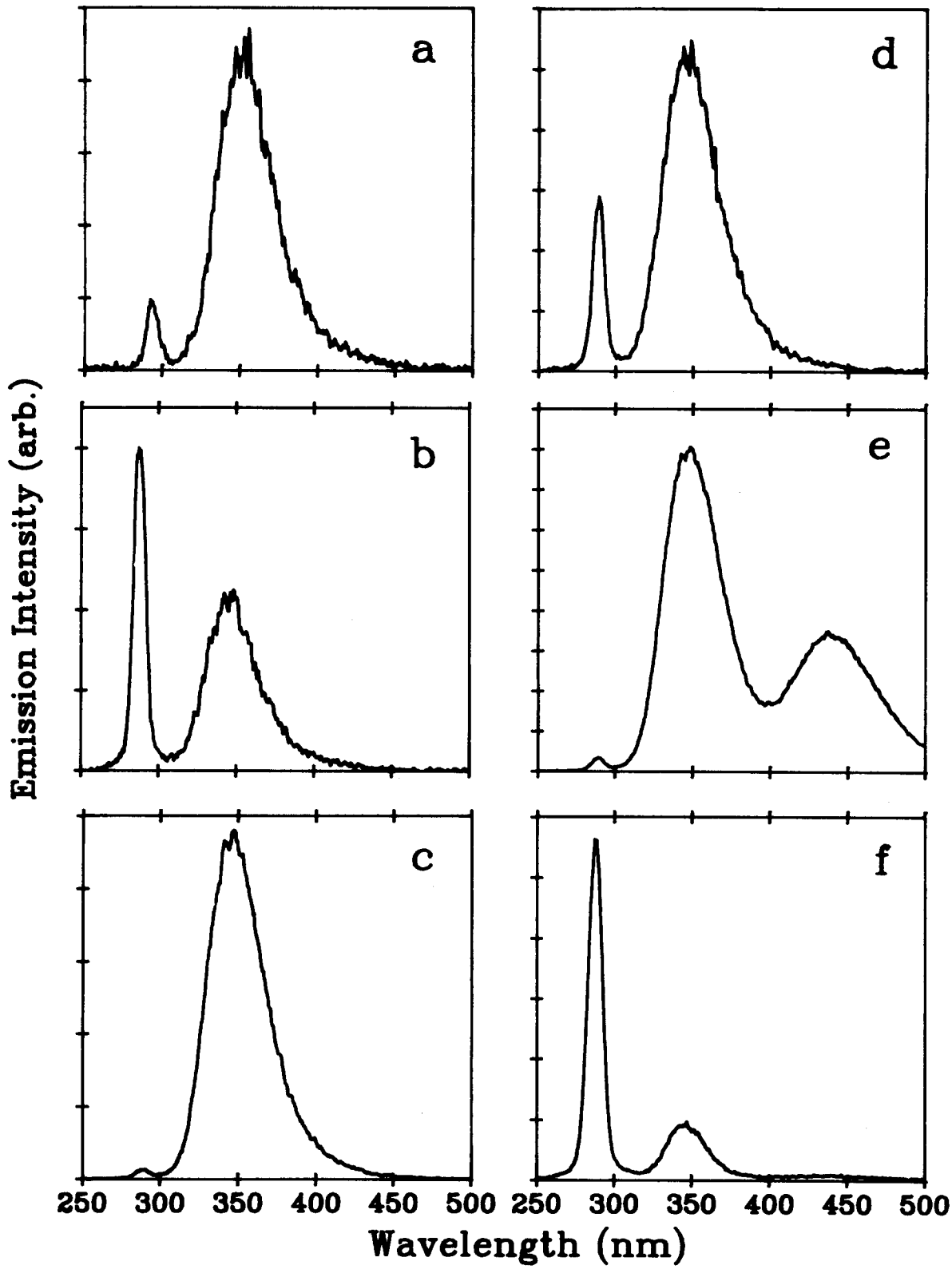

FIG. 9. Emission spectra from a multiply doped F_2:Kr:Xe/Ar solid, under different irradiation histories. For a detailed description, see Sec. III D. The narrow band at 285 nm corresponds to XeF($D \rightarrow X$), the broadband at 343 nm corresponds to $(ArKr)^+F^-$, the band at 439 nm in (e) corresponds to Kr_2F in Ar, the spectrum in (f) shows the XeF ($D \rightarrow X$) and ($D \rightarrow A$) bands only.

results.[11,12] It should be evident from the comparison that the excitation spectrum in the present is identical with the absorption spectrum reported by Ault and Andrews from their F:Kr:Ar matrices,[12] despite the fact that the emission monitored in our studies is absent in theirs. The implication of this observation is that for F atoms isolated in mixed Ar/Kr cages, the optically induced charge transfer leads to the diatomic configuration. Except for a large shift ($\sim$2500

TABLE I. Spectroscopic parameters for KrF($B \leftarrow X$).

v'	$E(\text{cm}^{-1})$	Relative intensity Expt.	Calc.
0	37 814	0.6007	0.6107
1	38 127	0.7905	0.7111
2	38 419	0.9675	0.9853
3	38 712	1.0	1.0
4	39 006	0.9595	0.9906
5	39 290	0.8343	0.8402
6	39 593	0.6779	0.6800
7	39 873	0.5437	0.4909

	This work	Ault and Andrews[a]	Gas phase[b]	Theory[c]
ω_e' (cm^{-1})	309 ± 10	315 ± 10	310	339
$\omega_e x_e'$ (cm^{-1})	2.28 ± 0.8	1.5 ± 0.5	1.21	1.7
T_e (cm^{-1})	$37\,700 \pm 10$	37 800	40 409	41 780
ω_e''	$75(\pm 3)$[d], $70(\pm 1)$[e]	50–100	130,[f] 33[g]	···
$r_e'' - r_e'$ (Å)	0.31	0.25	···	···
r_e'' (Å)	2.75	···	···	···

[a] Reference 12.
[b] Reference 34.
[c] Reference 35.
[d] Experiment.
[e] Molecular-dynamics simulation using pair potentials of Ref. 38.
[f] Estimated using pair potentials of Ref. 37.
[g] Estimated using pair potentials of Ref. 38.

cm^{-1}) in the electronic origin, the frequency and anharmonicity of the KrF(B) state is consistent with those of the gas phase. It would seem that, except for a vertical lowering of this ionic state, little else can be detected as a solid-state perturbation. It should, however, be remembered that the exciplexic potential is very deep, and that the properties measured here are sensitive only to the curvature of the ionic potential near its bottom.

In contrast with the deeply bound ionic excited state potentials, the ground-state interactions between halogens and rare gases are dominated by dispersive forces. The description of these weak interactions, and in particular their modification by many-body contributions, are of fundamental interest.[36] The rare-gas–halogen systems are particularly well suited for pausing such questions, since reliable pair potentials have become available for them from gas-phase molecular-beam data.[37,38] In addition, in the case of the KrF($B \leftarrow X$) transition, the distance-dependent transition dipole has been calculated.[35] Thus, from the Franck–Condon envelope of the KrF excitation spectrum in solid Ar, it should be possible to infer the projection of the ground-state wave function along the KrF coordinate. From such a wave function, the separation between excited- and ground-state minima, and the local frequency of the trapped F atom, can be obtained. To proceed, we evaluate the excitation intensities:

$$I_{\text{exc}} \propto \nu |\langle \psi_f(r) | \mu_{if}(r) | \psi_i(r) \rangle|^2 \qquad (2)$$

in which for the final state, the exact Morse wave functions are generated numerically (for a one-dimensional Morse function with parameters $D_e = 10\,469$ cm^{-1}, $\beta = 1.45$ Å^{-1}); for the distance dependence of the transition dipole, the curve given in Ref. 35 was fitted to a fourth-order polynomial (for 1.5 Å $< r <$ 4.2 Å, $\mu_{if}(r) = -126.3 + 170.8r - 80.55r^2 + 16.30r^3 - 1.208r^4$ for μ_{if} in debyes and r in Å); and for the initial state, trial wave functions are used. A good fit was obtained for a Gaussian of standard deviation $\sigma = 0.17(\pm 0.005)$ Å, and for a difference in potential minima, $r_e'' - r_e' = 0.31$ Å. If we then assume that this represents a wave function for the localized Kr–F vibration, a harmonic frequency of $75(\pm 3)$ cm^{-1} can be derived. The stick spectrum obtained from this set of parameters is shown in Fig. 2(a). The normalized transition moments are collected in Table I, and compared with the normalized experimental intensities. The overall variance between experiment and theory is 3% and there does not seem to be an obvious systematic deviation. Direct comparison of these parameters with gas-phase spectroscopic data is not possible, since gas-phase emission spectra are analyzed under the assumption that the KrF(X) potential is not bound.[34] Thus, we rely on the gas-phase pair potentials obtained from scattering data for the sake of making meaningful comparisons.

A meaningful comparison between the effective solid-state potential experienced by the F atom and gas-phase pair potentials is possible by comparing the experimentally determined F-atom frequency with that predicted under the assumption of pairwise additivity. To this end, we rely on classical molecular-dynamical simulations. The system and methodology are the same as those recently used for the simulations of F_2 photodissociation in crystalline Ar;[26] as such they will not be elaborated here. The most recently revised Kr–F pair potentials by Aquilanti *et al.*[37] are in significant disagreement with the earlier crossed molecular-beam re-

sults of Becker, Casavecchia, and Lee.[38] The former prescribe a potential minimum of 274 cm^{-1} at $r_e = 2.84$ Å, while the latter give a minimum of 56 cm^{-1} at $r_e = 3.01$ Å. The Ar–F pair potentials given by these authors are in better agreement. For the sake of completeness we have used both sets of parameters. However, it should be noted that the reliability of the Aquilanti potential for KrF is questionable, since it predicts a deeply bound X state with a Morse frequency of 133 cm^{-1} for which there is no evidence in the gas-phase emission spectra.[34] For the sake of computational convenience, we first fit all of the pair potentials to the Morse form.[26] A total of 366 atoms are used to simulate an fcc lattice of Ar, doped with one Kr and one F atom. The Kr atom is introduced as a substitutional dopant in the center of the cell. After imparting initial velocities randomly chosen from a 12 K Boltzmann distribution, the system is allowed to thermalize. The Kr–F internuclear separation is then monitored for several picoseconds, and its Fourier transform used to determine the local mode frequency. Since the simulation is strictly classical, the lattice temperature predetermines the range of the trap potential sampled by the F atom. However, we find that at the cryogenic temperatures of the studies, 4–50 K, the atoms sample a mostly harmonic lattice. Accordingly, the frequencies determined to within ± 1 cm^{-1} are insensitive to temperature in this range. While both substitutional and interstitial F atoms are considered, agreement between experiment and simulation is obtained only for the potentials of Becker, Casavecchia, and Lee, and for an F atom trapped in the O_h interstitial site neighboring the Kr atom. The results of this simulation are shown in Fig. 10. The time evolution of the Kr–F distance is shown in Fig. 10(a), in which a clear vibrational motion centered at an equilibrium distance of 2.75 Å, and with an amplitude of ± 0.1 Å, can be seen. A power spectrum of the same motion is shown in Fig. 10(b), in which a sharp, localized resonance can be seen at 70 cm^{-1}. Note that, in the potentials used here, the Morse frequency and r_e'' of the isolated Kr–F pair are 33 cm^{-1} and 3.01 Å, respectively. Thus the simulated values are those of the cage potentials, and as such are sensitive to the isolation site of the atom. A broadband ranging between 30 and 40 cm^{-1} is obtained for the frequency of an F atom trapped as a substitutional neighbor to Kr. The Aquilante potentials for the O_h trapped F atom yield a frequency of 155 cm^{-1}, in clear disagreement with the experiment.

Whether the $\sim 7\%$ discrepancy between simulation and experiment is due to the approximations made (such as the neglect of zero-point motions) or due to the assumption of pairwise additivity is not clear. A more detailed theoretical analysis does not seem warranted in the absence of more direct, such as Raman or IR, data on the ground-state frequencies. However, even at this level of sophistication, several conclusions can be safely made. We may conclude that the F atoms are trapped at interstitial O_h sites; and the simulated ground-state Kr–F equilibrium distance $r_e'' = 2.75$ Å should be reliable. Using the above determined difference between ground- and excited-state minima, an equilibrium distance $r_e' = 2.44$ Å is obtained for KrF(B). This value should be compared to the *ab initio* calculations of KrF(B) in the gas phase,[35] which predict an equilibrium distance of

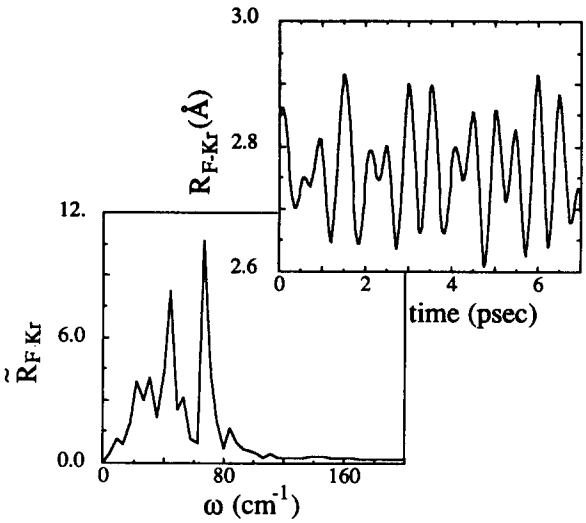

FIG. 10. Molecular-dynamics simulations of an F atom trapped at an octahedral site of an argon lattice, with one Kr nearest neighbor. The simulation contains 366 atoms in all, thermalized to the experimental temperature of 12 K. In the upper panel, the time evolution, for 7 ps, of the Kr–F internuclear separation is shown. In the lower panel, the Fourier transform of the same motion is shown, in which a transform-limited resonant mode at 70 cm^{-1} can be seen.

2.51 Å. Due to the dominant bound-free nature of the gas-phase emission spectra, it has not been possible to obtain a reliable experimental value for r_e'.

B. F/Kr emission

As in the case of solid Xe, single broad emission bands which can be directly correlated with the gas-phase triatomic exciplexes are observed in solid Kr doped with the different atomic halogens.[15(b)] In the case of solid Xe, the possibility that the emission is due to $Xe_n^+ Cl^-$ delocalized states has been disproved on both theoretical[5–7] and experimental[1,2] grounds. Stable delocalized states are expected to be even less important in the case of solid Kr, hence all of the arguments used in the case of Xe are even more valid for Kr. The assignment of the 453 nm emission band, shown in Fig. 3, to Kr_2F as opposed to a larger cluster, is further established in the multiple doping experiments discussed in connection with the ArKrF emission above. In F:Kr:Ar samples of 1:1:3000 this emission can be generated after induction of photomobility [see Fig. 9(e)], and destroyed after thermal cycling. Formation of Kr clusters is highly unlikely in such dilute solids, while dimerization is to be expected by random diffusion of hot atoms (see below). Finally, the observed line shape can quite adequately be analyzed using the known triatomic potentials. Since in what follows we will be interested in the kinetic energy released upon the radiative dissociation of exciplexes, analysis of the emission line shape is necessary to provide a quantitative description of the repulsive surface where the radiative transitions terminate.

Kr_2F has been studied both theoretically and experimentally in the gas phase.[39] Given the broad unstructured emission spectrum of the triatomic exciplexes, in general,

little detail is discerned from the experimental spectra. The theoretical description of these exciplexes has been successful in predicting absorption and emission profiles and intensities, and as such remains the most reliable point of reference. According to the *ab initio* calculations, the structure of the exciplex in the lowest state of the ionic manifold, in the $4^2\Gamma$ state, is that of an isosceles triangle, with a Kr–Kr distance of 2.77 Å, and a Kr–F distance of 2.67 Å.[40] Thus, the separation between the Kr atoms is substantially shorter than their van der Waals distance of 4.0 Å,[41] and very similar to that found in Kr_2^+, $r_e = 2.79$ Å.[42,43] Indeed the exciplex is regarded as a purely Coulombically bound Kr_2^+ and F^- ion pair. The breadth of the emission is due to the fact that the vertical transition leads to a strictly repulsive ground potential. It has previously been shown in the case of Xe_2Cl that the emission profiles can be reproduced by reflection of a two-dimensional Gaussian wave function (representing the Rg_2^+ and Rg_2^+–X^- as independent harmonic oscillators) from the repulsive potential composed of Rg–Rg and Rg–X pair potentials.[1] In the present case, such a treatment does not seem necessary since the contribution from the Kr–Kr coordinate alone would be predicted to be broader than the entire emission profile. However, a fairly good reproduction of the observed emission profile can be obtained by considering this coordinate with only minor perturbations. To demonstrate this, we simulate the expected vertical neutralization spectrum for $Kr_2^+ \rightarrow Kr_2$ by the one-dimensional reflection method. For the ground state, the exponentially repulsive potential derived from gas-phase scattering data is used without any alterations.[44] For the excited state a harmonic wave function for Kr_2^+ with its gas phase $\omega_e = 188$ cm^{-1} is used.[42,43] The electronic energy E_0 of the excited state is left as a free parameter to match the emission maximum, and the equilibrium distance of Kr_2^+ is varied to match the width. The simulated spectrum, for values of $E_0 = 3.9$ eV, and $r_e = 2.83$ Å [which is 0.04 Å longer than the theoretical value for Kr_2^+ in $Kr_2F(4^2\Gamma)$], is superposed on the experimental spectrum in Fig. 3. The agreement is quite acceptable, given the approximate nature of the treatment. However, the approximation can be justified by noting that at the theoretically determined equilibrium distance between Kr and F in Kr_2F, both KrF X and A potentials are rather shallow (-0.01 and 0.08 eV relative to ground, respectively), and therefore are not expected to add significant width to the emission of the triatomic exciplex. Better agreement should be possible by a multidimensional treatment of the reflection; however, the problem is underdetermined. While a unique determination of the excited-state geometry and force constants is not possible from the emission spectrum alone, it is possible to conclude that the emission profile is mostly determined by the Kr–Kr repulsion on the ground surface. Thus, the radiative dissociation of Kr_2F leads to creation of the neutral atoms ~ 1 eV above ground, and nearly all of that energy is initially released as repulsion between the two Kr atoms.

The electronic energy of 3.9 eV for the triatomic configuration, determined in the above presented analysis, should be quite reliable. Its accuracy is contingent upon the assumption that in the range of the distances sampled by the Kr_2^+ coordinate, the Kr–Kr potential is well represented by two-body potentials. Since this corresponds to a range of energies 1 eV above ground, and more than 1 Å contraction between a pair of Kr atoms, the assumption should be rigorously valid.

C. F/Kr excitation

Comparison of the excitation spectrum of F/Kr with that of F:Kr/Ar in Figs. 4 and 2, respectively, enables the assignment of the degraded band at 253 nm to the diatomic $B \leftarrow X$ absorption. The band at 236 nm is in the expected range for the $D \leftarrow X$ absorption of KrF. However, these are clearly minority components in the spectrum and the main excitation peak in this solid is at 275 nm—red shifted from the lowest diatomic resonance by ~ 0.2 eV. Since direct Franck–Condon access of the triatomic is not possible due to the more than 1.2 Å difference between the equilibrium separations of Kr–Kr distances in the ground and excited states, this excitation cannot be assigned to any known gas-phase charge-transfer complexes. Its assignment to a delocalized charge-transfer transition $Kr_n^+ X^-$ is inescapable.

Delocalized charge-transfer states of halogen-doped xenon have previously been treated in some detail. Two different limits have been considered: delocalization among nearest neighbors only,[5–8] vs the formation of truly extended states of the solid.[3,4] The formalism of diatomics in ionic systems (DIIS) was developed by Last and George for the first case, while the concept of Rydberg holes was advanced for the latter. Clearly the progression predicted by the Rydberg analogy is absent in the present excitation spectra even though they were expected to be stable in halogen-doped solid Kr. We note in this context that the two theoretical frameworks used for these interpretations are mutually exclusive. In the DIIS formalism, the delocalized state results from the overlap of atomic orbitals, and the band structure of the rare-gas valence holes is completely ignored. In the Rydberg treatment, the positive charge is treated as a valence hole with an effective mass that reflects the full valence bandwidth, and no provisions are made for specific electron correlations in the atomic basis set at the impurity site. Clearly, the two models attempt descriptions of limiting behaviors. In the absence of a more rigorous global treatment—one that incorporates both local and extended states—we are left with these simplified and therefore incomplete descriptions of the charge transfer states. In the present case the DIIS treatment, i.e., delocalization of the hole among only nearest neighbors, seems the more appropriate limit. This conclusion is reached based on the observed collapse of the expected Rydberg progression, and also based on the fact that charge separation could not be achieved in Kr doped with any of the halogen atoms—neither phosphorescence nor thermoluminescence is observed in F-, Cl-, or Br-doped solid Kr.

In the DIIS formalism, the charge-transfer states of the system are created by the overlap of the valence orbitals of the Rg_nX system, in which n represents the coordination number of the halogen which depends on the isolation site—12 for substitutional trapping, 6 for O_h, and 4 for T_d. The ground covalent states are due to the overlap of the p hole on the halogen atom (p_x, p_y, and p_z orbitals) with the closed-

shell rare-gas neighbors, while the excited ionic states are created by the overlap of the closed valence shell of the halide ion with the *p* hole on a given rare-gas neighbor, summed over all neighbors. As in the case of the treatment for a substitutionally isolated Cl in Xe, due to the mismatch in cavity and atomic sizes, in the case of F in Kr multiple peaks are to be expected.[7] Indeed, given the small size of F^- atoms ($r = 1.33$ Å), and the absence of very diffuse *p* holes in Kr, we would expect delocalization to be unlikely in substitutional sites (cavity radius equal to 4 Å). In these large cavities, the F atom is expected to remain near the cavity wall, and therefore as in the case of F in Xe the diatomic resonances are to be expected.[2] F atoms fit well in interstitial sites of Kr. In the undistorted interstitial O_h site the cavity radius is 2.82 Å, which is very close to the potential minimum of KrF(X), as discussed above. In the undistorted interstitial T_d site, the cavity radius is 2.4 Å, which although somewhat tight for the ground state, corresponds to the minimum of the ionic Kr^+F^- state as determined above from the analysis of KrF in Ar. Therefore, in these tight-fit ground-state sites, we may expect a single-excitation peak. Based on these considerations, a consistent interpretation of the observed spectra is possible. The weak diatomic bands are assigned to F trapped in either substitutional sites, or in sites in which delocalization is prohibited by the presence of a nearest-neighbor impurity or defect. This would also explain the observation of diatomic KrF resonances in absorption, and triatomic Kr_2F in emission in concentrated F:Kr:Ar matrices—in the absence of a complete shell of Kr atoms in contact with the F atom, delocalization is not possible. The main excitation peak in the present is then assigned to F in intersitial sites. A distribution of such sites, and significant variation of their relative populations, is to be expected based on the methods used for the preparation of the solids. For example, the absorption spectra reported previously for F/Kr in amorphous matrices show the sharp resonance flanked with a broad blue tail with extensive diatomic contributions.[11,12] In the present, F atoms are prepared in crystalline solids by photodissociation of F_2. In such solids, F_2 fits somewhat loosely in substitutional sites. In the case of symmetric dissociation (dissociation in which atoms exit the cage), both atoms are expected to be trapped predominantly in interstitial O_h sites—an expectation that has been repeatedly observed in all molecular-dynamical simulations of these systems.[26,45,46] In the case of asymmetric photodissociation one of the F atoms is left behind in a loose substitutional site. However, during extensive irradiation of the solids, due to the photo-induced mobility of F atoms, a dynamic equilibrium leading to the preferential population of the deeper interstitial sites at the expense of the looser substitutional sites is to be expected. Thus the main absorption at 275 nm is rather safely assigned to the octahedrally trapped F atoms, i.e., to $Kr_6^+F^-$.

Finally, an energy-level diagram for the different charge-transfer configurations in the F/Kr system can be constructed (see Fig. 11). From the excitation spectra of KrF in Ar and also the degraded diatomic origin in F/Kr, the energy of the diatomic charge-transfer configuration, Kr^+F^-, is obtained at 4.7 eV above ground. From the main

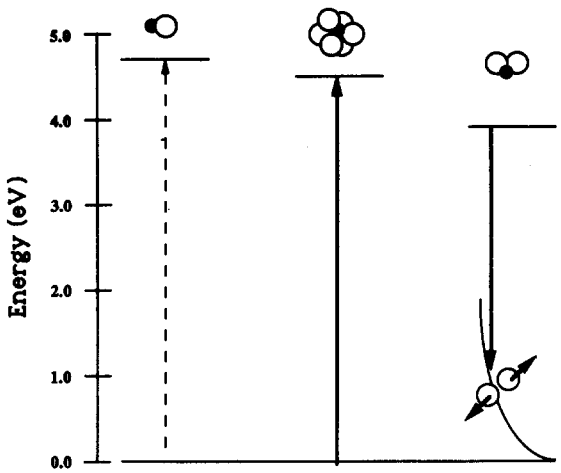

FIG. 11. Energy-level diagram for charge-transfer states in F/Kr. The charge-transfer state configurations are shown schematically (open circle, Kr; filled circle, F). The dashed arrow points at the diatomic charge-transfer state, Kr^+F^-, observed in excitation spectra of F/Kr:Ar and as a degraded spectrum in F:Kr solids. The excitonic state, with charge delocalization among nearest-neighbor Kr atoms is observed in excitation spectra, and the triatomic is observed in emission spectra in F:Kr solids. The triatomic emission terminates at 1 eV above ground; all of this energy is released as Kr–Kr repulsion.

excitation origin in F/Kr, the energy of the delocalized configuration $Kr_6^+F^-$ is obtained as 4.5 eV. This implies a resonance energy for delocalization of 0.2 eV. The energy of the triatomic state, 3.9 eV, was obtained above from the analysis of the Kr_2F emission spectrum. Therefore, the localization energy to the triatomic configuration, which can be regarded as the Jahn–Teller distortion of the symmetric cage, is obtained as 0.6 eV. Note that the difference in energies between the diatomic and triatomic charge-transfer configurations of 0.8 eV is closely related to the binding energy of Kr_2^+ of 1.05 eV.[42,43]

D. Photodissociation of F_2 in Kr

The photodissociation cross section, $\gamma = 1(\pm 0.1) \times 10^{-20}$ cm^2, for F_2 in solid Kr at 12 K, was measured by monitoring the growth rate of the F-atom concentration during 308 nm irradiation of the sample. The determination of the 308 nm laser fluence is the largest source of error in this measurement. Since the dissociation is carried out to completion, we can be sure that the cross section refers to molecules isolated in crystalline sites. The technique of dual delays in this measurement directly establishes that the F atoms probed are stable with respect to recombination for time scales 10 ns $< t <$ 50 ms. Upon completion of dissociation, insignificant recombination is observed in samples left overnight. In short, the photodissociation cross section is for the permanent cage exit of F atoms. The technique, however, does not allow the probe of geminate recombination on a subnanosecond time scale. The latter process is presumably responsible for the observed dissociation quantum yield of $0.5(\pm 0.1)$. This value is at least 5 orders of magnitude larger than the quantum yields for dissociation of Cl_2 and ICl under similar conditions.[47,48] Note, the quantum yield value

is based on the gas-phase absorption coefficient of F_2, and should be revised once a solid-state value is available. Such corrections are expected to be minor, and the conclusion that the photodissociation of F_2 is subject to only a minor cage effect will not change.

The photodissociation of F_2 via its repulsive $^1\Pi_u$ surface in solid Ar has recently been studied in some detail both experimentally and theoretically. These will be reported in forthcoming publications.[26,27,49] For the present, we note that experimentally, efficient dissociation is observed at all studied wavelengths, 450–250 nm, and the results are at least in qualitative agreement with the molecular-dynamical simulations. At 308 nm excitation, F_2 is borne with 2.4 eV of excess energy on its repulsive $^1\Pi_u$ surface. A quantum yield of 0.95 (subject to sampling errors of 14%) is predicted by the theory for this excess energy in solid argon.[26] A somewhat smaller cross section is to be expected in Kr due to its heavier mass. Thus, the present result is in accord with the molecular-dynamical results and support the details of the microscopics that have emerged from those studies.

E. Two-photon-induced harpooning of F_2

The two-photon-induced dissociation of F_2 is fascinating both for its implied mechanism and its inordinately large cross section, $3(\pm 2)\times 10^{-45}$ cm^4 s near 275 nm. This value was determined from two different measurements: the two-photon-induced growth kinetics, and the transmission measurements at high fluence in virgin F_2/Kr samples. The agreement between the two different measurements implies that, within experimental errors, the cage exit probability of F atoms upon the two-photon excitation is unity. This result is not too surprising in view of the fact that the cage exit probability via the standard photodissociation channel is also near unity. It has previously been established that in systems where direct photodissociation suffers a very large cage effect, e.g., Cl_2/Kr, Cl_2/Xe, Br_2/Xe, the two-photon-induced charge transfer leads to efficient photodissociation.[20] The concept of a "negative" cage effect,[2,20] and the charge hopping model,[21] have been offered to explain the efficiency of this solid-state photoinduced harpoon reaction. Given the simplicity of the electronic states in the present system, and the absence of competing two-photon absorption mechanisms—such as sequential two-photon mechanisms (see below)—it is possible to comment on the origin of the observed large absorption cross sections.

It is useful to compare the two-photon absorption cross section measured in the present to those of more familiar absorptions. The two-photon absorption cross section of Kr at 193 nm, in the gas phase, is 5×10^{-50} cm^4 s—which is a typical, large cross section for two-photon processes.[50] The same process has also been measured in solid Kr, and a cross section of 1×10^{-48} cm^4 s is obtained.[51] This enhancement could be explained by the fact that in the solid state, two-photon excitation at 193 nm leads to the conduction-band continuum above the gap [11.61 eV (Ref. 9)]. Charge-carrier generation by two-photon pumping has been demonstrated in solid xenon.[52] Thus, the two order of magnitude enhancement can be ascribed to the increased density of final states. In the present case, the measured cross section is 5–6 orders of magnitude larger than typical gas-phase two-photon processes, and therefore characteristic of resonance enhancement. In the case of F_2-doped Kr, at 275 nm the only intermediate-state resonance that exists is the $F_2(^1\Pi_u \leftarrow X)$ continuum. The energy of two photons at 275 nm is just below the first exciton of Kr [9.33 eV (Ref. 9)], and does not reach any known states of F_2 [the second continuum of F_2 starts above 10.4 eV (Ref. 53)]. Thus, the charge-transfer state which may be designated as Kr^+–F_2^- is the only candidate for the terminal state of the excitation. It is possible to estimate the energy of such a transition based on the observed charge-transfer band of F_2–Xe in liquid Xe, which peaks near 185 nm.[54] If we account for differences in ionization energy between xenon and krypton, then a broad resonance at $\sim$140 nm can be predicted for the analogous $Kr^+F_2^-$ in solid Kr. This is well matched with the energy of two photons at 275 nm. Such a band should be broad, and its exact description should include hole delocalization in Kr; however, here we will refer to this state simply as $Kr^+F_2^-$. The two-photon induced process then fits the harpoon description:[20]

$$Kr + F_2 + 2h\nu \rightarrow [Kr^+F_2^-] \rightarrow Kr^+F - + F, \qquad (3)$$

and its large absorption cross section has to be rationalized by the intermediate-state resonances:

$$F_2(X) + Kr + \left[\xrightarrow{h\nu} F_2(^1\Pi) + Kr \xrightarrow{h\nu}\right] Kr^+F_2^-. \qquad (4)$$

Note that in this scheme the second photon resonance gains its intensity from the $KrF(B \leftarrow X)$ transition. In addition to the fulfillment of the resonance conditions, two other considerations contribute to the enhancement of the cross section: (a) the two-electron nature of the transition—the first resonance promotes a molecular F_2 electron to a nonbonding state, while the second transfers a Kr electron to the excited molecule; and (b) the charge-transfer electron in the second resonance is from the valence band of Kr, and therefore a large density of states contributes to this final step. Even if we ignore the contributions from extended hole states in the final resonance, it is possible to argue that the charge-transfer electron may be derived from any of the Kr nearest neighbors, and therefore would have a degeneracy of 12. Therefore an oscillator strength much larger than unity is, in principle, possible. This in essence is the mechanism that leads to "giant two-photon absorptions" in excitonic molecules observed in such solids as the copper halides.[25]

This mechanism also explains the efficient two-photon generation of XeF in F_2:Xe:Ar solutions, and the successful demonstration of two-photon pumped liquid-phase laser action in that system.[55] Contributions from sequential two-photon pumping, e.g.,

$$F_2 + h\nu \rightarrow F_2(^1\Pi_u), \qquad (5a)$$

$$F_2(^1\Pi_u) \rightarrow F_2(^3\Pi_u), \qquad (5b)$$

$$F_2(^3\Pi_u) + h\nu + Kr \rightarrow + Kr^+F_2^-, \qquad (5c)$$

can be discarded in the present case based on the two-color experiments discussed in Sec. III. If indeed a long-lived intermediate state were present in the two-photon harpooning mechanism, which has been observed in the case of Br_2,[23] then in the experiments in which a 275 nm pulse follows the

308 nm pump, enhancement of the exciplex emission under the 275 nm pulse would have been expected. Although a negative result, these experiments clearly indicate that a sequential two-photon pumping scheme is not important in the case of F_2/Kr. An incidental conclusion is that the $F_2(^3\Pi_u)$ state, about which very little is known experimentally, is efficiently deactivated presumably undergoing rapid intersystem crossing to the ground electronic surface. The conclusion that the two-photon process is truly coherent, moreover that the intermediate state is a continuum state, seems best documented in the present studies. The present situation is analogous to the Cl_2–Xe two-photon harpooning near 4 eV, which has previously been measured to have a cross section of $\sim 10^{-45}$ cm^4 s in liquid Xe[20] and $\sim 10^{-43}$ cm^4 s in solid Xe.[2] Although much the same arguments were given there,[20] the possibility of sequential two-photon contributions could not be eliminated in a very satisfactory manner in those studies.

F. Transient absorption

One of the interests in the photodynamics of solid-state exciplexes is their potential as lasers. The photocycle in F-doped solid Kr, as in all X/Xe solids, fits the description of an optically pumped four-level laser. The optically pumped state relaxes on a time scale $t < 1$ ps to the triatomic Kr_2F state undergoing a large Stokes shift. The triatomic exciplex relaxes strictly by radiation, $\tau_r = 140$ ns, to the repulsive wall of the ground state. Thus the terminal state of the potential lasing transition is depleted on a subpicosecond time scale. The stimulated emission cross section σ_s for this transition can be estimated as

$$\sigma_s = n\lambda^4/(8\pi\tau_r c\Delta\lambda) = 8\times 10^{-18}\ \text{cm}^2, \qquad (6)$$

where $\lambda = 453$ nm is the emission band center and $\Delta\lambda = 63$ nm is the FWHM of the emission. Thus, at exciplex concentrations of 1:10 000 in solid Kr, superradiance is to be expected. We have failed to see any evidence of stimulated emission even though we estimate that under focused pumping conditions, the requisite number densities were attained. Instead, a transient loss at zero delay, with a cross section of 1.4×10^{-18} cm^2 was observed at 440 nm [see Figs. 8(b) and 8(d)]. This net loss should be interpreted as the difference between the stimulated emission cross section and the true loss cross section, whether the latter is due to absorption by the excited state or due to scattering. If we assume the former, then a very intense absorption by the triatomic exciplex of $\sim 10^{-17}$ cm^2 has to be assigned. Transient absorption studies in gas-phase Kr_2F have recently been reported.[56] At 440 nm, an absorption cross section of 2.4×10^{-18} cm^2 is observed and assigned to the $9\,^2\Gamma \leftarrow 4\,^2\Gamma$ transition. Despite this absorption, laser action on Kr_2F has been successfully demonstrated.[57] The fivefold enhancement of the transient absorption cross section relative to the gas phase could, in principle, be attributed to the expected excitonic nature of the manifold of excited charge-transfer states of Kr_2F. It would then be expected that the solid-state equivalent of the $9\,^2\Gamma \leftarrow 4\,^2\Gamma$ transition would be broad and intense, which would explain the lack of gain throughout the broad emission band of the triatomic exciplex in solid Kr. Similar observations have been made in recent studies of Cl-doped freestanding crystals of Xe.[58] It would therefore seem that this situation is fairly general, and therefore it may not be possible to observe laser action in solid-state triatomic rare-gas halide exciplexes. This negative result should be taken with caution; neither the nature nor the fate of the excited-state manifold of charge-transfer states is known at present. Finally, despite the fact that loss at zero delay is observed, the origin of this transient may not necessarily be due to optical absorption by the excited state. The energy released during the interconversion of the pump state to the triatomic configuration could, in principle, generate local defects that act as scattering centers. This point will be amplified below.

G. Transient scattering

The internal excitation of guests in solids will eventually decay into the phonon bath. The modes of decay into the bath, especially in the case of sudden release of energy far above the phonon spectrum of the solid, is of concern to photodynamical studies. As an example, in the case of photodissociation studies, the optical excitation could create fragments with initial energies of several eV. The fate of this excess energy is not well understood and is difficult to characterize even in theoretical simulations. In addition to multiphonon relaxation and subsequent rapid thermalization of the solid, the creation of shock waves, local melting, and destruction of the solid are all possible channels of dissipation. Evidence for all of these behaviors is observed in our pump-probe experiments. These are preliminary investigations of these processes, and while they have not yet been fully quantified, they do provide a phenomenological description.

The creation and subsequent transport and relaxation processes of nonequilibrium phonon populations in solids has been studies by various techniques.[59] One of the most common methods, and conceptually perhaps the simplest, is the temperature jump technique. In such studies, Joulean heat is transferred to the solid by passing a short burst of current through a wire attached to it, and the phonon pulses arriving at a bolometer mounted at opposite sides is monitored. In pure cyrstals, the time-of-flight spectrum is composed of sharp pulses, while in heavily doped crystals a broad distribution of arrival times is observed. The first type of behavior is referred to as ballistic phonons, and their flight velocities yield the speed of sound for the different branches of the phonon dispersion curves. The second type of behavior is due to a diffusive propagation, and can be treated by random-walk models in which upon scattering from defects a phonon of given frequency ω breaks down to create two at $\omega/2$. The latter mechanism is also the essence of thermal conduction in solids.[60] The transient loss profiles shown in Fig. 8 are quite similar to the time-of-flight spectra observed in the temperature jump studies, and are therefore interpreted by using the same terminology.

From the relatively sharp onset of the scattering loss transients, from which the speed of sound in Kr could be extracted, it is clear that a phonon front that propagates in the ballistic mode is being observed in these heavily doped polycrystalline solids. Such propagation is, however, limited

to lengths of ~0.5 mm. Within the excitation volume, of ~50 μm, purely ballistic propagation is also observed. However, in general, the sharp rise in the loss transient is followed by a tail which could, in principle, be fit to a $t^{-1/2}$ form, i.e., to diffusive decay into the bulk phonon bath. Given the limited signal-to-noise ratio of the present transients, no such fit is attempted; however, such an analysis could potentially be used as a direct measure of scattering rates (or lengths). Under strong pumping conditions, the acoustic front does not relax to the base line, instead it merges into a loss signal that lasts as long as milliseconds. The slow exponential recovery of the latter cannot be ascribed to cooling, but rather to the creation of scattering centers that become permanent when the pump power is further increased. When reversible, this process is equivalent to local melting and subsequent annealing. It is quite impressive to note that this reversible behavior is observed for pump powers as high as 300 MW cm^{-2}. An estimate of the energy density generated with focused, resonant excitation at 275 nm (longitudinal geometry) is useful for these analyses. Upon the radiative dissociation of Kr_2F, ~1 eV is released on the repulsive wall of the ground state. For a dilution of 1:4000, even if all F atoms were initially excited, this would result in the generation of 0.25 meV per atom (or equivalently a temperature jump of 2 K) in the pump volume, if the volume were fully thermalized. The observation of the shock waves and melting clearly demonstrate that this is a completely misleading consideration. The kinetic energy is initially impulsively released among the immediate neighbors of the isolation site. Momentum transfer in this step to the lattice atoms should be extremely efficient, since initially almost the entire recoil is in the Kr–Kr coordinate. Considering the cohesive energy of 0.116 eV per atom of solid Kr,[60] the initial impulse has sufficient energy to dislodge nearest neighbors from their lattice sites. Such defects in isolation could only contribute to isotropic Rayleigh scattering. Upon secondary collisions, shock waves are launched, which dissipate the excitation energy out of the excitation volume. The fact that ballistic propagation of these acoustic waves are observed, even though the solid is heavily doped and polycrystalline, implies that these correspond to long-wavelength phonons. The latter is further verified by the observation of group velocities near the speed of sound. Evidently, it is only after the launching of these shock waves that defects on the scale of the probe wavelength are formed. The latter relax on a time scale that is characteristic of atomic diffusion—a process that is vacancy assisted. Direct evidence for diffusion of F and Kr atoms in solid Ar, under hard pumping conditions, will be given below. However, since the F-atom concentration remains constant throughout the process, it is possible to conclude that heating is strictly localized to several nearest-neighbor shells of the excitation site. The latter conclusion is based on the fact that diffusion-controlled recombination of F atoms is observed at 17 K, i.e., only 5 K above the ambient temperature of the bulk.

H. Photoinduced mobility of F atoms

The photoinduced mobility of F atoms is illustrated in the multiply doped solids: solid Ar doped with F_2, Kr, and Xe. In order to understand the implication of the sequence of processes illustrated in Fig. 8, it is important to take note of the photodissociation and radiative dissociation channels available to the system at the two wavelengths of irradiation used—248 and 308 nm.

Independent of its trapping site, F_2 can undergo photodissociation at both wavelengths. The gas-phase absorption coefficients at 248 nm (1.5×10^{-20} cm^2) and 308 nm (2.1×10^{-20} cm^2) are similar. However, in the first case F_2 is created on its repulsive surface with 3.4 eV of excess energy, while the excess energy in the latter case is 2.4 eV. Since the dissociation quantum yield at 308 nm is 0.5, we may expect the quantum yield at 248 nm to be between 0.5 and 1. Once F atoms are photogenerated, they become transparent to irradiation at either of the wavelengths used if trapped in purely Ar cages. However, F atoms trapped near Xe or Kr sites can be optically excited.

In the case of F atoms, 308 nm can only induce the XeF($B\leftarrow X$) transition, i.e., it can only excite F atoms neighboring xenons. The excitation leads to population of both B and C states. The B state relaxes by the $B\rightarrow X$ bound-to-bound transition, while the C state relaxes via the $C\rightarrow A$ bound to repulsive emission. The latter transition terminates ~0.5 eV above ground, and nearly all of this energy is initially released as recoil of the F atoms.

F atoms trapped as neighbors of either Kr or Xe can be excited at 248 nm. In the first case the excitation leads to the formation of $(ArKr)^+F^-$, which subsequently undergoes radiative dissociation. An estimate of the kinetic energy released by this transition is possible in analogy with the analysis of the Kr_2F emission spectrum given above. The diatomic KrF(B) state is located at 4.7 eV, and the ArKrF emission band is centered at 3.9 eV. The difference between these two energies is the sum of the repulsive potential in the ground state and the stabilization energy of the triatomic relative to the diatomic. The latter value should be somewhat smaller than the binding energy of $ArKr^+$ of 0.59 eV.[61] Thus we may expect the mixed triatomic to radiate to ground-state repulsive surface, ~0.5 eV above ground. In the case of F atoms neighboring Xe, the XeF($D\leftarrow X$) transition is excited at 248 nm. XeF(D) subsequently relaxes by the two radiative channels $D\rightarrow X$ and $D\rightarrow A$. The $D\rightarrow A$ transition leads to kinetic-energy release of ~0.6 eV, again mostly as F-atom recoil. However, only 20% of the D population relaxes via this channel. The branching ratio between $D\rightarrow X$ and $D\rightarrow A$, and the excess energy on the A surface, can be inferred from Fig. 9(f).

The initial, zeroth-order growth of XeF and ArKrF emissions, by 248 nm irradiation, implies that most of the F atoms are photogenerated in the bulk of Ar, and find their ways to the Xe and Kr sites. If only F_2 molecules originally trapped near these sites were responsible for the growth, then we would expect exponential growth and saturation. Instead, a linear growth in emission intensities is observed after irradiation doses that would correspond to tenfold the saturation limit. At the end of this irradiation period, it is estimated that every xenon site is populated by a nearest-neighbor F atom. Moreover, the rate of growth of XeF centers is nearly twice that of KrF centers, even though the

Xe concentration in the solid is more than three orders of magnitude smaller than that of Kr. There are two obvious reasons for this effect: (a) XeF is deeply bound in its ground state, while the KrF and ArF ground-state potentials are very similar and essentially only bound by dispersive interactions; (b) 248 nm excitation leads to radiative dissociation of the ArKrF with sufficient kinetic energy released to induce mobility of F atoms away from the Kr center. Thus while Xe centers act as deep traps for F, only a photodynamic equilibrium can be established at Kr centers. A more subtle consideration that may be in effect is the possible role of distortion guided channeling of the F atoms toward the Xe and Kr centers. Due to the mismatch in atomic radii, we may expect lattice dilatation around these sites in crystalline Ar—distortions that radiate several shells away from the centers. It may then be expected that such defects may act as antennae for the photomobile F atoms. This effect should be greater for Xe than Kr, consistent with the observed larger trapping rate at Xe centers. This conjecture could, in principle, be tested by molecular-dynamics simulations.

Irradiation at 308 nm of the solids leads to a depletion of Xe centers, while the F-atom population at Kr centers grows. The increased trapping at Kr centers is consistent with the photodynamical steady-state argument advanced above. At 308 nm, while F_2 dissociates, KrF centers cannot be excited and hence cannot be depleted. The depletion of XeF centers has to be attributed to the kinetic energy release upon $C \rightarrow A$ radiative dissociation of the diatomic exciplex.

Perhaps the most impressive observation is the reversibility of this process after very extensive irradition of the solids. After irradiation periods that correspond to complete dissociation of F_2, Kr centers are populated at the expense of Xe when excited at 308 nm, and when we switch to 248 nm excitation the Xe centers are populated at the expense of Kr. This shuttling would imply very extensive migration of atoms upon the impulse of ~ 0.5 eV given to them in the radiative dissociation process. It is important to note that the shuttle is between completely isolated Xe and Kr sites. ArKrF emission cannot be induced at sites in which Kr and Xe are neighbors, and the XeF $D \rightarrow X$ emission undergoes a large shift between Ar and Kr. Since all Xe centers are populated by photodissociation and during the subsequent shuttle, the migration range of F atoms must be of the order of the average separation between Kr and F_2 centers of ~ 15 lattice sites. This length can be bridged by a relay as follows: After extensive irradiation of the solids, if we assume complete dissociation of F_2, then the Ar bulk contains an F-atom concentration of 1:1500. These centers are, however, not excited by the lasers. F atoms ejected from the Kr or Xe sites, after radiative dissociation of the exciplex, enter the Ar bulk where they may recombine to form F_2. The latter will then photodissociate, and the excess energy of photodissociation (> 2.4 eV) can generate mobile F atoms. These mobile atoms may then either reach a Kr or Xe site, or undergo recombination with F_2 to repeat the cycle. In order to observe reversible shuttling between Kr and Xe centers, in this relay mechanism it is necessry for the F atoms to travel on average a length determined by the F–F separations in Ar of ~ 10 lattice sites! Such long-range migration was previously postulated in solid Ar to explain the efficient production of XeF centers.[14] In recent molecular-dynamics simulations, migration of F atoms by 10 lattice sites in crystalline Ar was observed for initial impulses of ~ 1.2 eV per F atom (a photodissociation excess energy of 2.4 eV).[26] The migration is not diffusive, but rather a straight trajectory in which the F atoms are channeled by the Ar lattice. The present studies clearly establish the existence of extensive photomobility, and support the microscopics that have resulted from the molecular-dynamics simulations.

Given the unique signature of Kr_2F and Xe_2F emissions, their absence in spectra (a)–(d) of Fig. 9 implies that the dopant rare-gas statistics are for the most part probabilistic. The observation of Kr_2F centers only after irradiation of the solid with intensities near its damage threshold implies that indeed some local melting and diffusion of the Kr atoms has occurred. Given the very low Xe concentration, clustering of Xe atoms remains improbable. Finally, the warm-up cycle clearly indicates that while F atoms are mobile at Kr sites, they are deeply bound at Xe sites. Indeed upon dark warm-up, the emission from XeF centers increases. The latter effect can clearly be attributed to diffusion of F atoms in the Ar bulk, and their eventual trapping at Xe sites. This observation was also previously reported in the studies of the XeF($D \rightarrow X$) laser in solid Ar.[15]

V. CONCLUSIONS

Fluorine-doped rare-gas solids provide an ideal opportunity for the detailed characterization of a variety of elementary photoprocesses in solids. The sampling provided in this article included molecular dissociation, photon-induced migration of atoms, dark diffusion and recombination, charge-transfer energetics and dynamics, and final degradation of excess energies in the bulk phonon bath. Several important conclusions could be drawn about each one of these phenomena, even though clearly further investigation of each is warranted.

In the case of photodissociation of F_2 in solid Kr, it was shown that the process is subject to only a minor cage effect. The same also holds for dissociation in solid Ar, which will be elaborated in greater detail in a subsequent publication.[27] This observation should be contrasted with the nearly perfect cage effect observed in the case of Cl_2 under similar conditions.[47,48] The difference in quantum yields of dissociation between these two different halogens is larger than six orders of magnitude. These results are in qualitative accord with recent molecular-dynamical studies of these two systems. At cryogenic temperatures, no dissociation for Cl_2 even in Xe is observed,[45] while very efficient dissociation of F_2 is observed in crystal Ar.[26] Two other observations are in good accord between theory and the present experiments: the photogenerated F atoms undergo long-range migration upon the initial impulse, and trap exclusively in octahedral interstitial sites. The latter conclusion was derived in the present work by extracting the ground-state KrF vibrational frequency in solid Ar—which could only be rationalized as due to octahedrally trapped F atoms. Indirect evidence for the same conclusion was also obtained in the analysis of the charge-transfer excitation in F/Kr. The long range migra-

tion of ~ 10 lattice sites upon an initial impulse of ~ 1 eV per F atom is a nearly coherent process unique to the F/Ar system.[26] Its origins are clearly found in the interaction potentials and the relative masses of the projectile and host atoms; for a more detailed analysis of the microscopics of this process we refer readers to the discussion in Ref. 26. Finally, quantum yields of photodissociation of F_2 in both crystalline Ar and Kr as a function of temperature and excess energy have been recently measured. They will be reported with a more detailed comparison with theory.[27]

Two-photon-induced harpoon reactions of molecular halogens, and hydrogen halides in condensed rare gases, have previously been discussed in some detail. While convincing evidence has been given in some examples, e.g., HCl/Xe,[1] and ICl/Xe,[62] for the coherent nature of the photoabsorption, in most cases this conclusion is reached by indirect arguments[20] and competing mechanisms can be shown to be present (e.g., Br_2/Xe and Cl_2/Xe).[23] In the case of F_2/Kr, the coherent nature of the two-photon excitation could be demonstrated, the cross section for the two-photon excitation could be directly measured (3×10^{-45} cm^4 s), and the transition uniquely assigned to an excitonic upper state with an intermediate resonance in the molecular $^1\Pi_u$ continuum. Furthermore, it was demonstrated that this process also leads to photogeneration of F atoms in the solid with near-unity quantum yield. This mechanism also provides a more satisfactory explanation for the observed efficient two-photon generation of XeF in liquid Ar.[55]

The two vertically accessed charge-transfer excitations described in this paper, F/Kr and F:Kr/Ar, display behavior intermediate in relation to those previously catalogued in the literature. In the case of the single-host F/Kr system, excitation leads to a partially delocalized state—delocalization among immediate neighbors. This is only possible in tight interstitial sites, and the preponderance of evidence points at the octahedral trapping site. The state is therefore assigned to $Kr_6^+F^-$. The DIIS formalism provides an appropriate theoretical framework for describing this state.[5–8] However, it is pointed out that existing treatments describe only limiting behaviors and therefore lack predictive power. A global treatment of these charge-transfer excitations, treatments that include both local and extended states of the solid, is highly desirable. In the case of the mixed host system, F:Kr/Ar, delocalization effects are completely eliminated and the diatomic exciplex KrF(B) is accessed in vertical transitions. However, this state is only metastable—it relaxes on a time scale of 20 fs $< t <$ 500 fs to the mixed triatomic configuration, namely $(ArKr)^+F^-$. In this context it should be pointed out that in the case of F/Xe, the diatomic $D\leftarrow X$ and $B\leftarrow X$ envelopes have been observed and fitted by a Franck–Condon analysis.[2] This state subsequently delocalizes as evidenced from charge separation and energy-storage observations.[3] Based on the present analysis of interconversion time scales, and the absence of any vibrational resolution in the vibronic envelope in F/Xe, it is possible to conclude that the diatomic states there decay on the time scale of $t < 20$ fs. Thus in both cases, the diatomic charge-transfer state undergoes an extremely efficient interconversion to the triatomic configuration, and the latter relaxes radiatively.

An analysis of the Kr_2F emission profile was given. While a unique fit could not be obtained, it was possible to conclude that the minimum of this molecular charge-transfer state is located at 3.9 ($\pm$0.1) eV, and that it relaxes to the repulsive wall of the ground state 1($\pm$0.1) eV above ground. Most of the repulsive energy release in this case is along the Kr–Kr coordinate. With the direct observation of diatomic KrF resonances, in both solid Ar and in loose sites in Kr, and the delocalized states in F/Kr, it was possible to give an energy-level diagram for the system. This is depicted in Fig. 11. The resonance energy for delocalization in going from the diatomic Kr^+F^- to the Frenkel-type $Kr_6^+F^-$ state is 0.2 eV. The localization of the latter, by breaking the spherical symmetry for the hole state, leads to a gain of 0.6 eV. This latter process is akin to a Jahn–Teller distortion associated with the local lattice relaxation. The relaxation of the system to this lowest-energy charge-transfer configuration occurs on a subpicosecond time scale, and is accompanied by the attractive release of $\sim$0.8 eV energy into the lattice. The final radiative relaxation of the triatomic results in the sudden release of ~ 1 eV of repulsive energy into the lattice. An analysis of the Kr_2F emission profile indicates that this energy is almost entirely released as repulsion along the Kr–Kr coordinate. The Kr–Kr bond in the triatomic state is compressed by a ~ 1 Å relative to the ground-state nearest-neighbor distance in solid Kr. Thus the excitation-emission photocycle in this case can be regarded as a means of generating a very-well-defined impulse in the solid. The subsequent response of the lattice to this dramatic perturbation was probed by the transient scattering experiments.

The impulsive energy released in the solid is dissipated by several mechanisms: the creation of shock waves, the creation of defects, and mass transport were observed. The effective propagation of the shock waves in a ballistic mode minimizes the jump in local temperature. With the direct observation of diffusive phonon propagation (or equivalently, relaxation into the equilibrium thermal bath), it is possible to conclude that thermal relaxation is complete on the time scale of $\sim 10^{-6}$ s. Annealing of defects, however, proceeds on time scales as long as $\sim 10^{-3}$ s. It is impressive to note that these crystals heal reversibly for pump powers as high as 300 MW cm^{-2}. In addition to the photon-induced long-range migration of F atoms, which as stated above is thought to be a very special case, under intense irradiation conditions the migration of Kr atoms in Ar were also demonstrated. This process is clearly mediated by vacancies created along with other defects upon the impulsive release of excess energies much above the Debye limit of the solid. Finally, we note that the experimental methods used for recording of these transients can be greatly improved by averaging techniques, and by using continuous wave probe beams. Such an approach would enable investigations of these phenomena with greater spatial resolution and under much milder pumping conditions. Such studies are presently underway.

As to the origins of the prompt transient loss, which prevents the triatomic exciplex from undergoing stimulated emission, a satisfactory answer could not be provided. It was

originally assumed to be due to an optical absorption by the exciplex. However, based on the spatial dependence of its time evolution, the main source of the loss is to be attributed to scattering. Spectroscopy of the excited state and improved transient loss studies could resolve this rather important issue.

ACKNOWLEDGMENTS

This research was supported by the U. S. Air Force Astronautics Laboratory under Contract No. F04611-87-K-0024. Grants made available to H. Kunttu by the Jenny and Antti Wihuri Foundation and the Alfred Kordelin Foundation are gratefully acknowledged.

[1]M. E. Fajardo and V. A. Apkarian, J. Chem. Phys. **85**, 5660 (1986).
[2]M. E. Fajardo and V. A. Apkarian, J. Chem. Phys. **89**, 4102 (1988).
[3]M. E. Fajardo and V. A. Apkarian, J. Chem. Phys. **89**, 4124 (1988).
[4]N. Schwentner, M. E. Fajardo, and V. A. Apkarian, Chem. Phys. Lett. **154**, 237 (1989).
[5]I. Last and T. F. George, J. Chem. Phys. **86**, 3787 (1987).
[6]I. Last and T. F. George, J. Chem. Phys. **87**, 1183 (1987).
[7]I. Last, T. F. George, M. E. Fajardo, and V. A. Apkarian, J. Chem. Phys. **87**, 5917 (1987).
[8]I. Last and T. F. George, J. Chem. Phys. **89**, 3071 (1988).
[9]N. Schwentner, E. Koch, and J. Jortner, *Electronic Excitations in Condensed Rare Gases*, Vol. 107 in Springer Tract in Modern Physics (Springer-Verlag, New York, 1985).
[10]I. Ya. Fugol, Adv. Phys. **27**, 1 (1978).
[11]B. S. Ault and L. Andrews, J. Chem. Phys. **65**, 3075 (1976).
[12]B. S. Ault and L. Andrews, J. Chem. Phys. **65**, 4192 (1976).
[13]J. Goodman and L. E. Brus, J. Chem. Phys. **65**, 3808 (1976).
[14]N. Schwentner and V. A. Apkarian, Chem. Phys Lett. **154**, 413 (1989).
[15](a) A. I. Katz, J. Feld, and V. A. Apkarian, Opt. Lett. **14**, 441 (1989); (b) V. A. Apkarian, in Proceedings of Lasers '89, New Orleans, Society for Optical and Quantum Electronics, edited by K. Duke (Bolt, Alexandria, 1990).
[16]H. C. Brashears, D. W. Setser, and Y. C. Yu, J. Chem. Phys. **74**, 10 (1981).
[17]E. I. Rashba, in *Excitons*, edited by E. I. Rashba and M. D. Sturge (North-Holland, Amsterdam, 1982), Chap. 13; E. I. Rashba, in *Defects in Insulating Crystals*, edited by V. M. Tuchkevich and K. K. Shvarts (Springer-Verlag, New York, 1981).
[18]Y. Toyozawa, in *Vacuum Ultraviolet Radiation Physics*, edited by E. E. Koch, R. Haenzel, and C. Kung (Pergamon, New York, 1974).
[19]I. Ya. Fugol, Adv. Phys. **37**, 1 (1988).
[20]M. E. Fajardo, R. Withnall, J. Feld, F. Okada, W. Lawrence, L. Wiedeman, and V. A. Apkarian, Laser Chem. **9**, 1 (1988).
[21]R. B. Gerber, R. Alimi, and V. A. Apkarian, Chem. Phys. Lett. **158**, 257 (1989).
[22]D. L. Andrews and K. P. Hopkins, Adv. Chem. Phys. (to be published).
[23]W. G. Lawrence and V. A. Apkarian, Israel. J. Chem. (in press).
[24]D. C. Cartwright and P. J. Hay, J. Chem. Phys. **70**, 3191 (1979).
[25]M. Ueta, H. Kanzaki, K. Kobayashi, Y. Toyozawa, and E. Hanamura, *Excitonic Processes in Solids*, Vol. 60 in Springer Series in Solid State Sciences (Springer-Verlag, New York, 1986), Chaps. 2 and 3.
[26]R. B. Gerber, R. Alimi, and V. A. Apkarian, J. Chem. Phys. (in press).
[27]J. Feld, H. Kunttu, and V. A. Apkarian (unpublished).
[28]W. Rudnick, R. Haensel, H. Nahme, and N. Schwentner, Phys. Status Solidi (a) **87**, 319 (1985).
[29]H. Kunttu and V. A. Apkarian (unpublished).
[30]R. B. Steunenberg and R. C. Vogel, J. Am. Chem. Soc. **78**, 901 (1956).
[31]D. S. Kupperman and R. O. Simons, J. Phys. C **4**, L5 (1971).
[32]R. Burnham and S. K. Searles, J. Chem. Phys. **66**, 1306 (1977).
[33]To obtain the solid-state radiative lifetime of KrF(B) in Ar, the relationship $\tau_s = 9\tau_g/n(n^2+2)^2$ is used. This has been previously successful in predicting diatomic lifetimes in RGS. For an original derivation, see R. L. Fulton, J. Chem. Phys. **61**, 4141 (1974).
[34]J. Tellinghuisen, A. K. Hays, J. M. Hoffman, and G. C. Tisone, J. Chem. Phys. **65**, 4473 (1976).
[35]T. H. Dunning, Jr. and P. J. Hay, J. Chem. Phys. **69**, 134 (1978).
[36]For a recent discussion, see J. H. Kim, T. Ree, and R. H. Ree, J. Chem. Phys. **91**, 3133 (1989), and references therein.
[37]V. Aquilanti, E. Luzzatti, E. Pirani, and G. G. Volpi, J. Chem. Phys. **89**, 6165 (1988).
[38]C. H. Becker, P. Casavecchia, and Y. T. Lee, J. Chem. Phys. **70**, 2986 (1979).
[39]D. L. Huestis, G. Marowsky, and F. K. Tittel, in *Excimer Lasers*, edited by Ch. K. Rhodes, Vol. 30 in Topics in Applied Physics (Springer-Verlag, New York, 1984).
[40]W. R. Wadt and P. J. Hay, J. Chem. Phys. **68**, 3850 (1978).
[41]J. A. Barker, R. O. Watts, J. K. Lee, T. P. Schafer, and Y. T. Lee, J. Chem. Phys. **61**, 3081 (1974).
[42]W. R. Wadt, J. Chem. Phys. **68**, 402 (1978).
[43]P. M. Dehmer and J. L. Dehmer, J. Chem. Phys. **69**, 125 (1978).
[44]C. Nyeland and J. P. Toennies, Chem. Phys. Lett. **127**, 172 (1986).
[45]R. Alimi, R. B. Gerber, and V. A. Apkarian, J. Chem. Phys. **89**, 174 (1988).
[46]R. Alimi and R. B. Gerber, J. Chem. Phys. **91**, 1611 (1989).
[47]V. E. Bondybey and C. Fletcher, J. Chem. Phys. **64**, 3615 (1976).
[48]V. E. Bondybey and L. E. Brus, J. Chem. Phys. **65**, 620 (1975), **64**, 3724 (1976).
[49]H. Kunttu and V. A. Apkarian (in preparation).
[50]See, for example, Ref. 39, p. 237.
[51]T. Kessler, R. Markus, H. Nahme, and N. Schwentner, Phys. Status Solidi (b) **139**, 619 (1987).
[52]E.-H. Böttcher and W. F. Schmidt, Phys. Status Solidi (b) **126**, K165 (1984).
[53]E. A. Colbourn, M. Dagenais, A. Douglas, and J. W. Raymonds, Can. J. Phys. **54**, 1343 (1976).
[54]M. E. Fajardo, V. A. Apkarian, A. Moustakas, H. Krueger, and E. Weitz, J. Phys. Chem. **92**, 357 (1988).
[55]M. Shahid, H. Jara, H. Pummer, H. Egger, and C. K. Rhodes, Opt. Lett. **10**, 448 (1985).
[56]D. B. Geohegan and J. G. Eden, J. Chem. Phys. **89**, 3410 (1988).
[57]F. K. Tittel, M. Smayling, W. L. Wilson, and G. Marowsky, Appl. Phys. Lett. **37**, 862 (1980).
[58]N. Schwentner and V. A. Apkarian (unpublished).
[59]W. E. Bron, in *Dynamical Properties of Solids*, edited by A. A. Maradudin in G. K. Horton (North-Holland, Amsterdam, 1990).
[60]See, for example, C. Kittel, *Introduction to Solid State Physics*, 5th ed. (Wiley, New York, 1976).
[61]C. Y. Ng, P. W. Tiedemann, B. H. Mahan, and Y. T. Lee, J. Chem. Phys. **66**, 5737 (1977).
[62]F. Okada, L. Wiedeman, and V. A. Apkarian, J. Phys. Chem. **93**, 1267 (1989).